Tip Extensions, Winglets, and C-wings: Conceptual Design and Optimization

S. Andrew Ning* and Ilan Kroo†
Stanford University, Stanford, CA, 94305

Conceptual wing design analysis methods are combined with numerical optimization to find minimum drag wings subject to constraints on lift, weight, pitching moment, and stall speed. Minimum drag tip extensions and winglets are compared using nonlinear optimization. The minimum drag trapezoidal tip device depends on the ratio of the maneuver lift coefficient to the cruise lift coefficient, although the difference in performance is small. The importance of accounting for the depth of the wing structural box in the weight model, and including constraints on stall speed are highlighted. C-wings are investigated for their potential to enhance performance beyond that offered by wings with winglets. C-wings are found to be a reasonable design alternative for tailless aircraft with requirements for nose-up pitching moment about the aerodynamic center. This may be especially true for span-constrained or low sweep designs. Optimizing C-wing designs introduces several subtleties into the optimization process including the necessity of evaluating the maneuver load at various lift coefficients, and constraining the wing skin thickness. Finally, the method is applied to wings with active load alleviation. Active load alleviation allows reductions in drag on the order of 15%, however further analysis of the structural dynamics is necessary to more fully quantify the results.

Nomenclature

AR	aspect ratio
b	span
c	chord
C_L	lift coefficient
c_l	section lift coefficient
C_{mac}	pitching moment coefficient about the aerodynamic center
c_r	root chord
c_t	tip chord
c_{avg}	mean geometric chord
D	drag
D_i	induced drag
h_{wlet}	height of winglet
I_b	bending weight index
J	objective
L	lift
ℓ	length
M_b	bending moment
n	load factor
q	dynamic pressure
S	wing area
t	thickness
t/c	thickness to chord ratio

*Ph.D. Candidate, Department of Aeronautics and Astronautics, AIAA Student Member.
†Professor, Department of Aeronautics and Astronautics, AIAA Fellow.

t_s	skin thickness
V_∞	free-stream velocity
V_s	stall speed
W	weight
y	spanwise coordinate

Subscripts

max	maximum
mvr	maneuver
ref	reference

Symbols

α	angle of attack
Λ	quarter chord sweep
λ	taper ratio
ϕ	dihedral angle
ρ	density
σ	bending stress
θ	local twist angle
ξ	coordinate tangent to wing

Matrices

$[AIC]$	aerodynamic influence coefficient matrix
$[D2]$	viscous drag influence coefficient matrix - quadratic term
$[DIC]$	induced drag influence coefficient matrix

Vectors

$\{\gamma\}$	circulation vector
$\{bc\}$	boundary condition vector
$\{c_l\}$	section lift coefficient vector
$\{CLIC0\}$	c_l influence coefficient vector - constant term
$\{CLIC1\}$	c_l influence coefficient vector - linear term
$\{D1\}$	viscous drag influence coefficient matrix - linear term
$\{LIC\}$	lift influence coefficient vector
$\{MIC\}$	pitching moment influence coefficient vector
$\{WIC\}$	weight influence coefficient vector

1. Introduction

High fuel costs and environmental concerns provide continuing motivation for research aimed at increasing aircraft efficiency. Vortex drag is a major contributor to aircraft drag, typically accounting for about 40% of the drag in cruise and about 80-90% of the drag in second segment climb.[1] Since vortex drag is strongly affected by wing tip geometry, wing tip optimization has received a great deal of attention because of its potential for reducing vortex drag. Improved wing tip design can benefit new designs and can be used to improve performance by retrofitting existing wings.[2]

One of the early wing tip modifications was a simple end plate.[3,4] These end plates were shown to increase the effective span of the wing, thus reducing the vortex drag. Richard Whitcomb at NASA achieved greater gains in efficiency through carefully designed high aspect ratio end plates which he termed winglets. His experimental data published in 1976 showed that a winglet improved the lift to drag ratio by nearly a factor of two as compared to a tip extension.[5]

Heyson et al. at NASA soon followed with a computational study in which a larger number of winglets and tip extensions were compared. The conclusion again was that "for identical increases in bending moment, a winglet provides a greater gain in induced efficiency than a tip extension."[6] In the following year (1978) Flechner and Jacobs conducted wind tunnel studies on four different jet transport configurations and found that the "ratios of relative aerodynamic gain to relative structural weight penalty for winglets are 1.5 to 2.5 times those for wing-tip extensions."[7] Again, the weight measurement used was root bending moment.

In 1980 Jones and Lasinski of NASA performed a computational study comparing tip extensions and winglets with a different weight constraint. They constrained integrated bending moment and found that for ideal wings, either a tip extension or a winglet provided essentially the same reduction in induced drag.[8] In 1984, Kroo also came to a similar conclusion using a weight model that accounted for the depth of the structural box and an aerodynamic model that included viscous drag.[9]

In the following year, Asai also performed a computation study with viscous drag, but with root bending moment as the weight constraint. He concluded that tip extensions provided a slight improvement over winglets.[10] In 1987 Zimmer conducted a theoretical and experimental study showing that triangular planar tip extensions were superior to nonplanar tip devices.[11] His weight computation involved a combination of root bending moment and planform area, but only induced drag was considered. A recent numerical study (2008) by Slingerland and Verstraeten included viscous drag, but used root bending moment as the weight constraint. Their findings were that winglets were only optimal for wings with span constraints.[12] This study also addressed C-wings and found no real aerodynamic benefit to using C-wings over wings with winglets.

There are several reasons why a reexamination of the relative benefits of tip extensions and winglets was warranted. First, the structural constraint used in most of these studies was root bending moment. Root bending moment does not account for the effect of chordwise changes in the planform on the bending weight. Root bending moment can be especially inappropriate for nonplanar configurations. Large winglets can be designed with zero or even negative changes in root bending moment. Also, most previous studies apply the weight constraint at the cruise lift coefficient. However, the lift distribution at cruise and at the critical structural condition can be quite different.

Second, many of these studies compare only induced drag. Including viscous drag can be particularly important when comparing tip extensions and winglets as the designs often have very different wetted areas. Fixing the wetted area does not allow for fair comparison between planar and nonplanar wings, neither does fixing the projected area.

Third, all of these studies analyzed a small number of designs, or parametrically varied a few of the design variables. Trade studies can be useful, but only cover a very limited subset of the design space. Wings with tip devices introduce more planform variables than can be handled properly by simple trade studies. In particular, many of the above mentioned studies used simple linearly extrapolated tip extensions. Such a tip extension is an ineffective use of wetted area for the same reason why an end plate is less effective than a winglet. Optimization was employed in some of the previous studies, but was limited to optimizing the lift distribution. Nonlinear optimization of the geometry is often required to properly compare these designs.

The present study seeks to address these concerns, and yet still retain simplicity in the analysis methods, as appropriate for conceptual design studies. Certainly, the choice of a tip extension, winglet, or other tip device depends upon many other considerations not addressed here such as the effect on the aircraft dynamics, aeroelastics, and even marketing. Our objective in this paper is not to design an airplane, rather we seek to explore fundamental, but complex multidisciplinary considerations in the design of wings and wing tip devices. Results are intended to show the importance of various assumptions and design degrees of freedom. We will not conclude whether winglets or tip extensions are "better". This would require a specific and complete aircraft design study.

We begin by exploring trade studies for planar wings, highlighting some of the modifications to the structural weight model. Next, we conduct trade studies for wings with tip extensions and wings with winglets. Tip extensions and winglets are then more formally compared using nonlinear optimization. C-wings are then investigated to determine if there are significant performance advantages to C-wing designs as compared to wings with winglets. Finally, the method is applied to wings with active load alleviation demonstrating a broader class of problems that can be handled in this conceptual design framework.

2. Method

2.1. Aerodynamic Model

Vortex drag is calculated at the Trefftz plane by using a drag free wake leaving the trailing edge of the wing planform. Viscous drag is calculated at each panel by assuming a parabolic variation in viscous drag coefficient with section lift coefficient. Changes in loading with twist and angle of attack are computed using a discrete vortex Weissinger model.[13] Two hundred control points are used, equally spaced along the wing semi-span. In some nonlinear optimization problems fifty panels across the wing semi-span are used. The details of the basic problem formulation are described by Kroo.[9] A few additions to this method were used,

as described in the following sections.

2.2. Weight Model

A few modifications are made to the structural weight model. First, we consider that the cruise lift coefficient is often different from the lift coefficient at which the critical structural load is reached. For example, many transport aircraft have their maximum maneuver load factor set at 2.5 as per FAR Part 25.[14] This maximum load factor is where critical loading occurs, and thus affects the amount of material needed to support bending loads. While the maximum load factor may be the same for many different aircraft, the critical maneuver altitude (or maneuver dynamic pressure) is not. Thus, the bending weight should be computed at the maneuver lift coefficient (C_{Lmvr}) and not the cruise lift coefficient. A derivation of the modifications made to the bending weight computation is available in the Appendix. As shown in the Appendix, the critical parameter to be specified is the ratio C_{Lmvr}/C_L.

Second, we consider variations in area-dependent weight. For most problems the wing area is held constant, so that the wing weight is assumed to be proportional to the bending weight. This is a good approximation for wings of moderate to high aspect ratios where differences in shear-dependent weight are negligible, and for wings with low to moderate sweep where differences in torsion-dependent weight are negligible. We do not examine wings of low aspect ratio or high sweep in the present paper, although in some cases, the wing area is allowed to vary requiring an assessment of area-dependent weight.

The wing weight can be decomposed into a part due to the load, and a part due to the size of the wing.

$$W = W_{load} + W_{area}$$

We assume that the load dependent weight is proportional to the weight of material used to resist bending loads, and that the area-dependent weight is proportional to the gross area of the wing.

$$W = k_1 I_b + k_2 S$$

where $I_b = \int \frac{M_b}{t} ds$ integrated over the wing semi-span, and k_1 and k_2 are appropriately chosen constants. A wing weight estimate of this form correlates well with the data from actual transport aircraft.[16] In this paper we are only interested in computing the ratio of weight to the reference weight, which leaves only one undetermined coefficient.

$$\frac{W}{W_{ref}} = \frac{k_1 I_b + k_2 S}{k_1 I_{b_{ref}} + k_2 S_{ref}} = \frac{I_b + k_W S}{I_{b_{ref}} + k_W S_{ref}}$$

where $k_W = k_2/k_1$. The value of this constant was determined by correlating actual aircraft data with the bending index used here.

2.3. C_{Lmax} Model

Stall speed is given by:

$$V_s = \sqrt{\frac{2L}{\rho S C_{Lmax}}}$$

A constraint on stall speed is important when optimizing the planform geometry. Without this constraint, optimization often leads to unrealistically small tip chords with high section lift coefficients. We require that all designs have a stall speed less than or equal to that of the reference wing. Since we have a fixed lift, this gives the inequality constraint $C_{Lmax} S \geq (C_{Lmax} S)|_{ref}$.

C_{Lmax} is difficult to predict and is really a three dimensional, unsteady, viscous phenomena. Consistent with the simplicity of our linear aerodynamic model developed so far, we use a simple method to estimate C_{Lmax}. We will use critical section theory to predict stall. Essentially, this means that stall is predicted when any one section of the wing reaches a specified section $c_{l\,max}$. Since we are not modeling any high-lift devices, we are constraining the clean wing stall speed.

This constraint on stall speed is not directly imposed in the optimization problem. For a given wing area the required C_{Lmax} can be found directly from the constraint $C_{Lmax} S \geq (C_{Lmax} S)|_{ref}$. The constraint imposed in the optimization problem is that at C_{Lmax} the c_l distribution must be less than or equal to a specified $c_{l\,max}$ ($\{c_l\}|_{C_{Lmax}} \leq \{c_{l\,max}\}$.).

As a side note, the vector $\{c_{l_{max}}\}$ need not correspond to actual airfoil section maximum lift coefficients. For example, in designing a wing with ailerons at the wingtips, it may be desirable to provide an outer panel c_l margin at the stall condition to account for aileron deflection and spanwise boundary layer flow. In this case a lower $c_{l_{max}}$ constraint might be used at the outer panels. With an actual airfoil $c_{l_{max}}$ larger than that specified by the constraint, the wingtips would have some margin against stall. However, in the results shown in this paper $c_{l_{max}}$ is constant across the wing for simplicity in discussing the results.

2.4. Optimization

Three different optimization methods are used, depending on the problem formulation. For the trade studies, the lift distribution is optimized to minimize total drag subject to various linear constraints. The use of a quadratic objective with linear equality constraints allows the optimal solution to be computed efficiently from a system of linear equations by using the method of Lagrange multipliers.[9]

The next set of problems continue to optimize the lift distribution, but with a constraint on stall speed. The section $c_{l_{max}}$ constraints are inequality constraints, and thus the method of Lagrange multipliers no longer leads to a simple system of linear equations. Since we must use a different solution method that allows inequality constraints, we can also relax the equality constraints on lift and weight. This does not change the optimal solution since the lift and weight constraint are both active at the minimum drag solution, but can allow the optimization to be more efficient. It does change the solution for designs with smaller spans than optimal. With an equality constraint on weight, the wing tips must be intentionally loaded up to increase the weight, making the performance of these wings appear worse than necessary. However, near the optimum, and for larger wing spans the weight constraint is always active.

We can now specify the optimization problem for $\{\gamma\}$ as follows:

$$\begin{aligned} \min \quad & \{\gamma\}^T[DIC + D2]\{\gamma\} + \{D1\}^T\{\gamma\} \\ \text{w.r.t.} \quad & \{\gamma\} \\ \text{s.t.} \quad & \{LIC\}^T\{\gamma\} \geq L_{ref} \\ & \{WIC\}^T\{\gamma\} \leq W_{ref} \\ & \{CLIC1\} \circ \{\gamma\} + \{CLIC0\} \leq \{c_{l_{max}}\} \end{aligned}$$

(The derivation of $\{CLIC1\}$ and $\{CLIC0\}$ is included in the appendix). Although we no longer have a simple system of linear equations to solve, this is still a straightforward quadratic programming problem with linear constraints. Further, it can be shown that it is a convex problem. To prove this, we only need to show that $[DIC + D2]$ is positive definite. This is trivial for $[D2]$ since it is a diagonal matrix with positive entries. The other quadratic term $\{\gamma\}^T[DIC]\{\gamma\}$ is equal to the induced drag, and in steady flow the induced drag of the system will be greater than or equal to zero. Thus the matrix $[DIC]$ must also be positive definite. The sum of two positive definite matrices is also positive definite, making this a convex problem. The convex programming problem is solved with `CVX`, a package for specifying and solving convex programs.[17,18]

The last set of problems involves changing the planform geometry as well as the lift distribution. Including the planform variables as design variables makes both the objective and the constraints nonlinear. These problems are solved using the sequential quadratic programming method. Specifically, MATLAB's *fmincon* was used to generate the results shown in this paper.

3. Trade Studies

In this section we optimize the lift distribution for a given geometry. Since we are not optimizing the geometry, the constraint on stall speed is not yet necessary. This allows for rapid solution of a system of linear equations. We will first explore some of the basic design trades and how different constraints affect the optimal solution. We will then perform some basic trade studies for wings with tip extensions and wings with winglets. The reference wing used in these calculations is a straight wing with elliptic loading. All designs have a fixed wetted area, and a fixed t/c of 0.12.

3.1. Weight Constraint

The classic minimum drag solution for a wing with fixed span is an elliptic distribution of lift. However, we are often not really interested in constraining the span, but rather constraining the weight. The resulting optimal lift distribution and reduction in drag depends upon the method used to estimate the structural weight of the wing.[19–22] For design studies, this is often done by estimating the weight of the wing required to resist bending. As mentioned previously, this is a good approximation for wings of moderate to high aspect ratio, low to moderate sweep, and fixed gross wing area.

Perhaps the simplest method to compare the bending weight of two wing designs is to compare the root bending moment. R.T. Jones obtained analytical solutions for the minimum induced drag of a straight wing with fixed lift and fixed root bending moment.[20] After some simplification the expression becomes:

$$\frac{D_i}{D_{i\ ref}} = 8\left(\frac{b_{ref}}{b}\right)^4 - 16\left(\frac{b_{ref}}{b}\right)^3 + 9\left(\frac{b_{ref}}{b}\right)^2$$

where the reference wing is elliptically loaded. Our computational results agree with this analytical solution (Figure 1). The conclusion is that a 15% reduction in induced drag can be achieved compared to an elliptically loaded wing with a 15% increase in span. Larger span increases do decrease the drag, but not significantly.

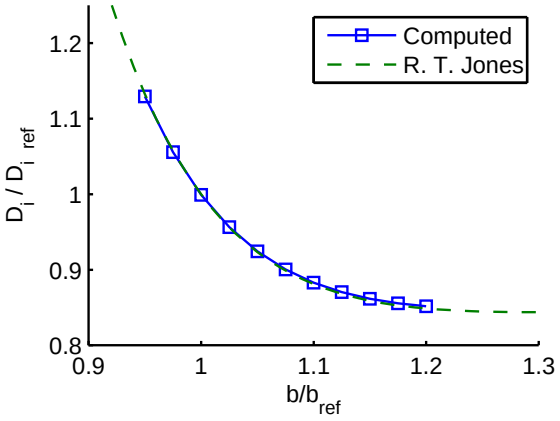

Figure 1. Comparison between computational results and R.T. Jones' analytic expression for minimum induced drag at a fixed root bending moment

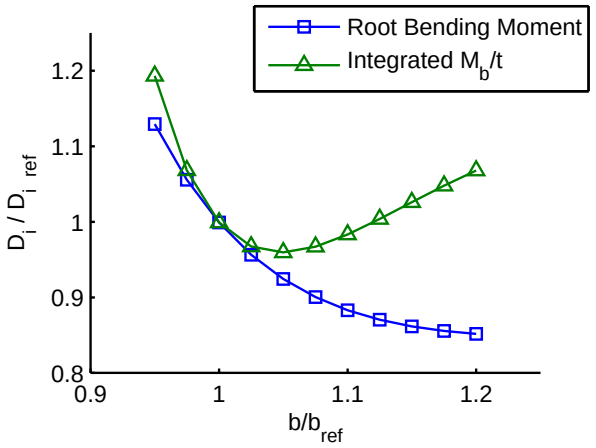

Figure 2. Comparison between two different methods for computing wing bending weight

Root bending moment, however, is not the most accurate indication of wing bending weight. A winglet, canted inward such that its generated lift vector passes through the wing root, would add zero root bending moment. One could create arbitrarily large winglets which would apparently produce no increase in weight. While the example may seem a bit contrived, root bending moment can be a poor prediction of bending weight for even very simple wings. The weight model used in this analysis accounts for the volume of material needed to resist bending loads.[9] Using this model, the conclusions change quite drastically. Figure 2 compares the results from using root bending moment with the more accurate integrated bending moment over thickness to represent weight.

We see that the two methods are very similar for spans close to the reference span, but deviate greatly for larger spans. This discrepancy is primarily due to the fixed area constraint. As we increase span at a fixed area, the chords decrease. For a fixed t/c distribution the wing thickness also decreases making the wing less effective in resisting bending. This reduction of the wing structural box is not accounted for in root bending moment considerations alone. Of course, if one wanted to increase the span significantly, one would probably increase the wing area as well and the drag penalty would not be as bad as shown here. The important point, however, is that root bending moment does not capture chordwise variations in the planform geometry which affect the depth of the wing structural box.

Using this more accurate weight model leads us to a different conclusion for minimum drag. It seems that for this wing the minimum drag occurs with a 5% increase in span, and only reduces induced drag by about 4%.

Let us consider the load distribution for this wing. Figure 3 shows the lift distribution for this case with a 5% increase in span compared to the elliptic lift distribution. We can see that for the higher span the

load has shifted inboard. This allows a higher span (with less induced drag) while still maintaining the same bending weight.

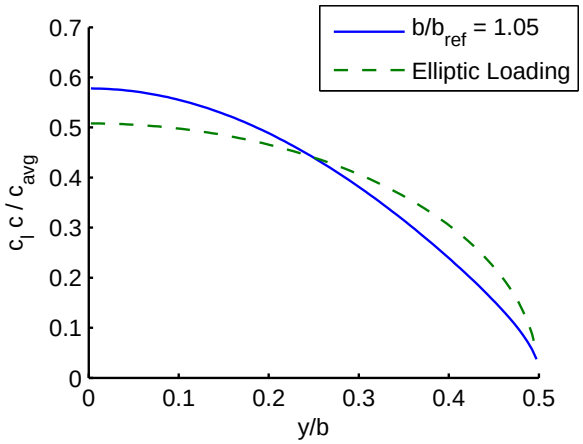

Figure 3. Optimal loading vs. elliptic loading

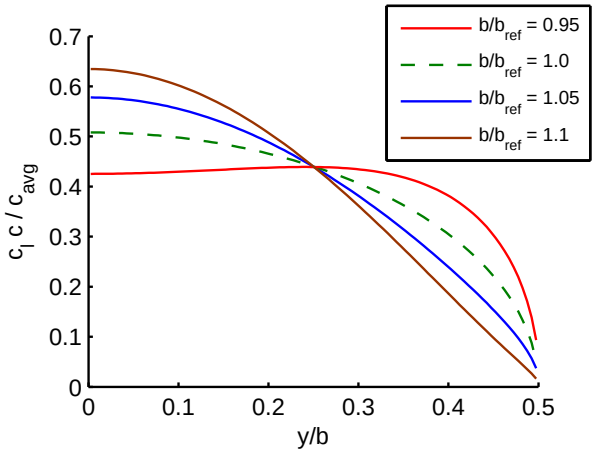

Figure 4. Load distributions for various spans

Figure 4 compares the loading distribution for two additional span lengths. We can see that at larger spans the lift distribution must be shifted farther inboard to meet the weight constraint. Although the span is larger, the efficiency is so poor that induced drag increases. Smaller spans do increase the induced drag, but the effect is exaggerated in this problem. This is due to the use of an equality rather than an inequality constraint for weight. This forces the wings with small spans to intentionally load up the tips, and creates unnecessarily poor span efficiencies. The use of an equality constraint, does not however affect spans near to or larger than the optimum.

We now add one additional consideration in the weight model. As mentioned previously, the wing's critical maneuver lift coefficient is often not the same as the cruise lift coefficient. For a given aircraft, the ratio of C_{Lmvr}/C_L depends upon the critical altitude. If the load factor is 2.5 and the critical maneuver load is obtained at cruise altitude then $C_{Lmvr}/C_L = 2.5$. If the critical maneuver load is reached at a lower altitude (higher q) then C_{Lmvr}/C_L is also lower. For example, if cruise was at 35,000 ft then, at constant Mach number, a C_{Lmvr}/C_L of 1 occurs at around 14,000 ft. In the following analyses we compare wings designed at a C_{Lmvr}/C_L of 1 and 2.5 to represent a range of possible designs with different critical structural altitudes.

For this simple straight wing, the minimum induced drag solution is now shown for the case where $C_{Lmvr}/C_L = 2.5$ (Figure 5). We can see that with a higher C_{Lmvr}/C_L this wing becomes very inefficient at larger spans. It appears that for this unswept untapered wing with $C_{Lmvr}/C_L = 2.5$, an elliptic lift

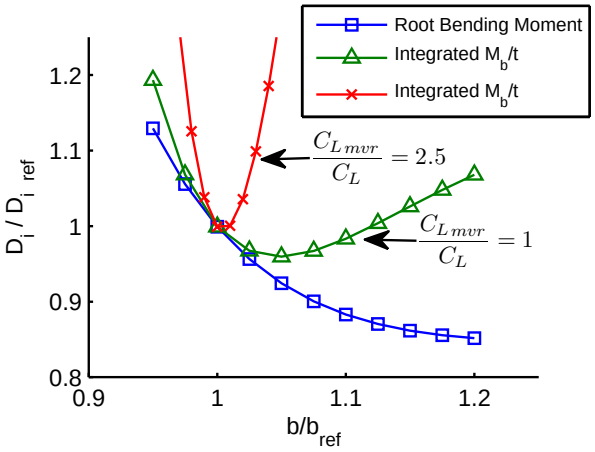

Figure 5. Variation in minimum drag solution with different weight constraints

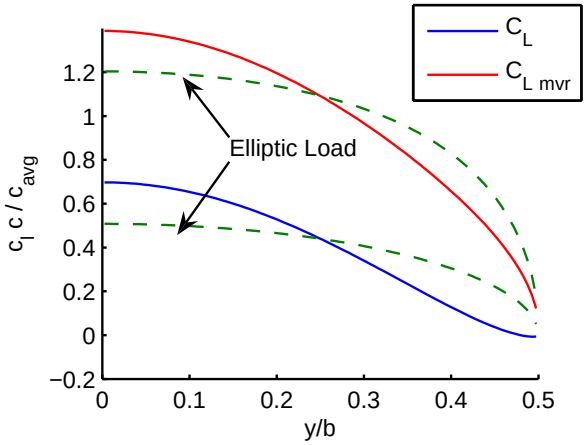

Figure 6. Optimal loading - large washout required ($C_{Lmvr}/C_L = 2.5, b/b_{ref} = 1.05$)

distribution really is the minimum drag solution. Of course, this geometry is clearly non-optimal. A tapered

wing should help to reduce the tip-loading and allow us to increase our span to achieve greater reductions in drag.

Let us also examine the lift distribution of this wing with $C_{L_{mvr}}/C_L = 2.5$. Figure 6 compares an elliptic lift distribution to the optimal lift distribution for a wing with a 5% span increase. This span increase is chosen because, as shown previously in Figure 2, for $C_{L_{mvr}}/C_L = 1$ this is the optimal span. The shifting of the load distribution inboard at $C_{L_{mvr}}$ looks qualitatively the same as we saw before. However, this is problematic because our cruise C_L is much lower. At lower angles of attack the basic lift distribution contributes more to the total lift distribution and the washout is more pronounced. In fact, in this case there is even a small section of downloading at the tips.

3.2. Viscous Drag

The above discussion on trading span and span efficiency focused on minimizing induced drag. We now include viscous drag calculations in the optimization. As discussed previously, the viscous drag calculation is modeled by assuming a parabolic variation with section lift coefficient. If we consider the drag polars of many different airfoils at a set of given flight conditions, we can fit a parabola through the minimum of all of the individual drag polars. This parabola represents minimum drag airfoils as a function of c_l. This means that we do not need to choose specific airfoils at this stage, but rather assume that appropriate airfoils will be used in each section that minimize drag at the local section c_l.

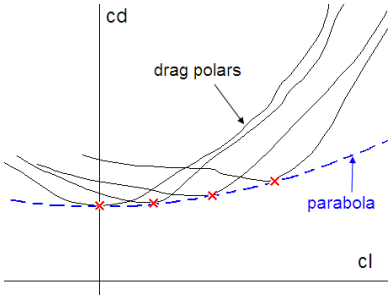

First, let us re-examine the case where $C_{L_{mvr}}/C_L = 1$ (Figure 7). Again, these results are for an untapered unswept wing.

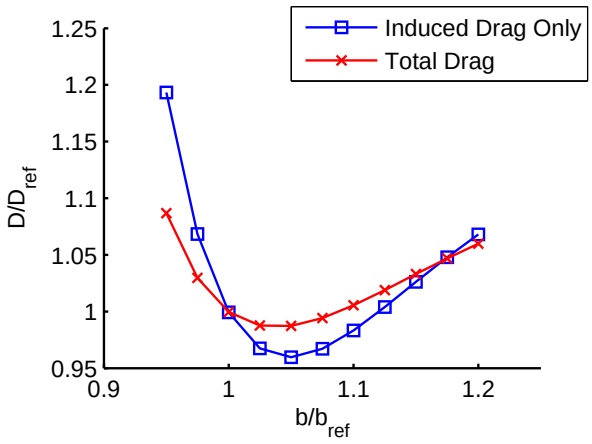

Figure 7. Comparison between induced drag only and total drag ($C_{L_{mvr}}/C_L = 1$)

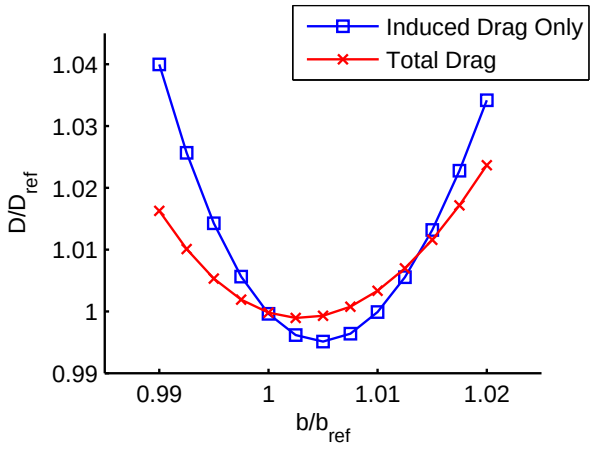

Figure 8. Comparison between induced drag only and total drag ($C_{L_{mvr}}/C_L = 2.5$)

The minimum drag is still at about a 5% increase in span, but the drag savings is down to around 2%. As one would expect, viscous drag accounts for about half of the total drag so the reduction in induced drag has about half of the effect it had previously. At $C_{L_{mvr}}/C_L = 2.5$ the results are similar. However, in this case the span of the reference wing is already very nearly optimal.

Including viscous drag often does little to affect the optimal span. However, viscous drag is a significant fraction of total drag, and is particularly important to include if the total wetted area is allowed to vary. From here forward every result will include viscous drag.

3.3. Taper

The results shown so far have been for an untapered wing. Adding taper can help alleviate some of the tip loads, requiring less washout at the critical structural load.

We will begin as before with the weight constraint applied at the cruise C_L. Figure 9 shows that decreasing the taper ratio can dramatically improve our drag savings. For a wing of taper ratio 0.1, we see a reduction

in drag of nearly 12% at a span increase of 20%. Since there is no constraint on section lift coefficient yet, for taper ratios smaller than 0.1 the drag does continue to decrease although the benefit is small.

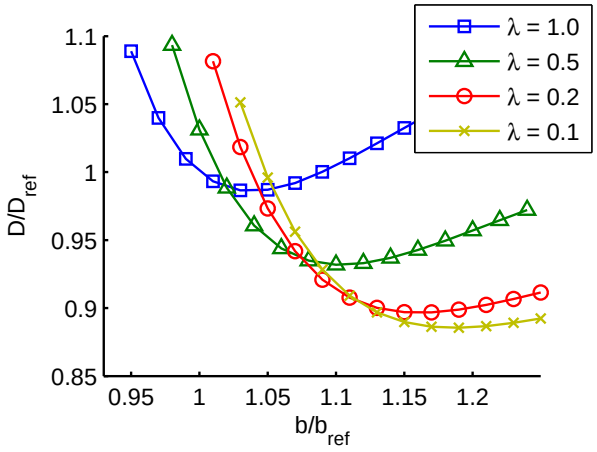

Figure 9. Minimum drag wings with various taper ratios

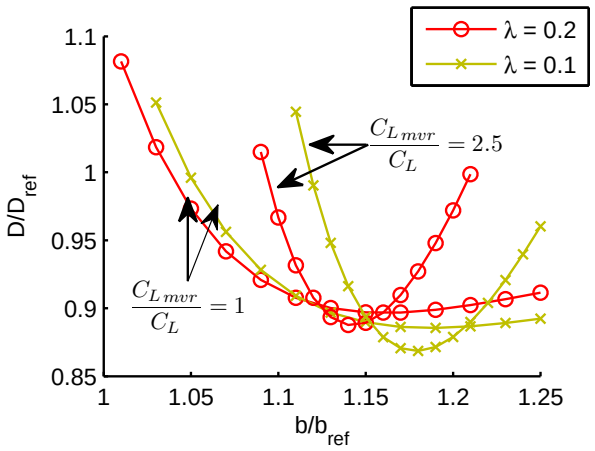

Figure 10. Minimum drag wings with various taper ratios and maneuver lift coefficients

Figure 10 compares wings with taper ratios 0.2 and 0.1 at $C_{Lmvr}/C_L = 1$ and $C_{Lmvr}/C_L = 2.5$. Wings designed with a higher C_{Lmvr}/C_L show some drag reduction relative to the wings designed with the maneuver lift coefficient equal to the cruise lift coefficient. We see that in this case the taper ratio 0.1 wing can achieve a drag reduction of nearly 14% at a span increase of 18%.

Let us look at the load distribution to determine why this is. Figure 11 shows the load distribution for the minimum drag case in the previous figure ($\lambda = 0.1$, $C_{Lmvr}/C_L = 2.5$, $b/b_{ref} = 1.18$). The low taper ratio decreases the lift toward the tip, allowing the wing to meet the structural weight constraint without the need for much washout. Thus, the load distribution at the cruise C_L is nearly elliptical as seen in the figure.

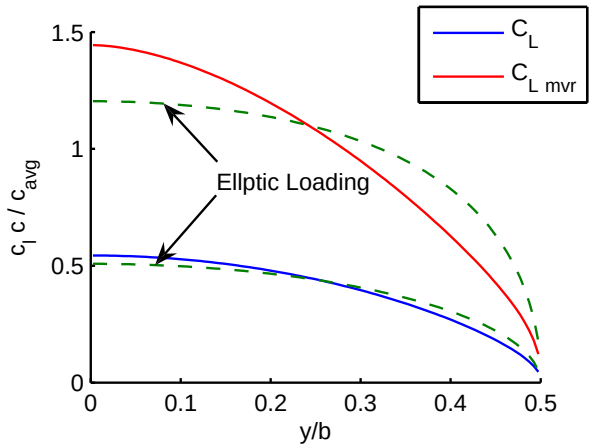

Figure 11. Optimal loading - little washout required ($\lambda = 0.1$, $C_{Lmvr}/C_L = 2.5$, $b/b_{ref} = 1.18$)

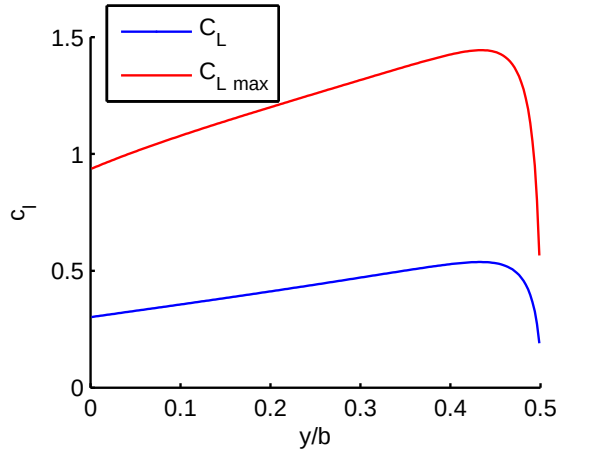

Figure 12. Corresponding c_l distribution at cruise and C_{Lmax} - low taper ratios may lead to poor stall performance

For this tapered wing, the drag is dramatically reduced, but the stall performance may be undesirable. Figure 12 shows the c_l distribution at cruise and at C_{Lmax}. We have seen that decreasing the taper ratio further will also decrease the drag further. However, smaller tip chords will lead to even larger section lift coefficients. When performing planform optimization, stall constraints are necessary to prevent unrealistically high section lift coefficients. This will be considered in more detail in a later section.

3.4. Tip Extensions

We now examine some basic trade studies for tip extensions. The main wing is unswept, the length of the tip is 10% of the wing semi-span, and C_{Lmvr}/C_L is set at 2.5. The taper ratio, from tip chord of the tip

extension to root chord of the main wing is 0.2.

First, we vary the sweep of the tip extension (Figure 13). In this case tip sweep is allowed to vary from 0° to 60°. For comparison, the curve for the unraked tip is the same as the curve in Figure 10. We see that there is some drag reduction for highly swept tips (raked tips). Results are similar for $C_{L_{mvr}}/C_L = 1.0$, but the drag reduction is less.

Previously, we saw that low taper ratios were desirable for unloading the wingtips, but that small tip chords led to poor cl distributions. Raked tips are beneficial for unloading the tips without reducing the tip chords significantly. However, the high sweep at the tip invalidates our assumption of neglecting torsion-dependent weight. Thus, subsequent planform optimization problems will limit sweep.

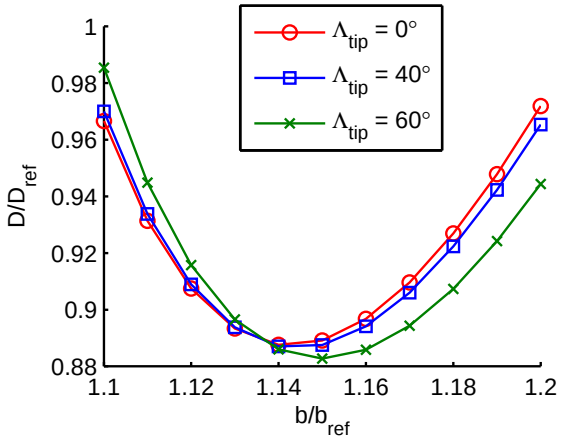

Figure 13. Variations in sweep of tip extension for a 0.2 taper ratio wing

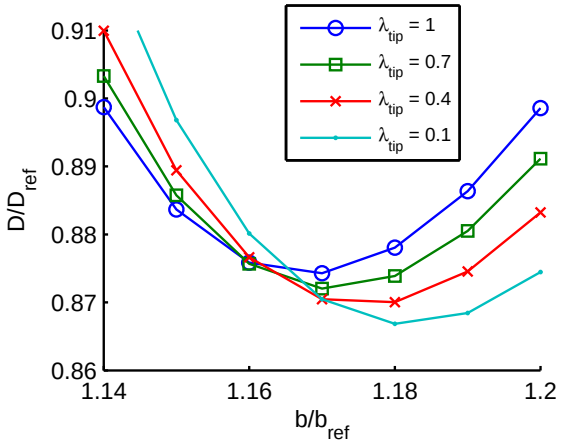

Figure 14. Variations in taper ratio of tip extension for a 0.2 taper ratio wing

Figure 14 shows the effect of changing the taper ratio of the tip. The main wing taper ratio is fixed at 0.2 and the sweep of the tip extension is fixed at 40°. As expected, small taper ratios for the tip extension also help to reduce drag.

The drag reductions in the previous figures are not large, but this is not to suggest that raked tips or other tip extensions offer no significant improvements. Assessing the benefits of multi-parameter variations requires nonlinear optimization and will be addressed later.

3.5. Winglets

Nonplanar wings open up a variety of possibilities. In this section we explore simple vertical winglets. We begin by examining untapered unswept wings. All winglets in this section are also untapered and unswept. Figure 15 and 16 vary the winglet height for $C_{L_{mvr}}/C_L = 1$ and 2.5 respectively. From both figures we see that increasing the height of the winglet decreases the optimal wingspan as one would expect. However, the winglets show an increase in drag as compared to the planar wing. For a 20% winglet the optimal span decreases by 12% but the drag increases by 3.5%. At $C_{L_{mvr}}/C_L = 2.5$ the trends are similar but with slightly different values. A 20% winglet now has a 10% lower optimal span and 3% more drag.

Now let us make the same comparisons for a tapered wing. Figures 17 and 18 show the same variations in winglet height for a $C_{L_{mvr}}/C_L$ ratio of 1 and 2.5 respectively. The wing has a taper ratio of 0.2 but the winglet is still vertical, untapered, and unswept.

For the $C_{L_{mvr}}/C_L = 1$ case we see that a 10% winglet has negligible penalty for drag and allows a 5% reduction in span. This seems to suggest that for tapered wings, winglets may only be useful for aircraft with gate constraints. For the $C_{L_{mvr}}/C_L = 2.5$ case, however, we can see a drag benefit from the larger winglets. For a 20% winglet we have a 1-2 % reduction in drag and a 7% decrease in span.

Finally, let us assess the effect of changing winglet dihedral angle. Results are shown for the same wing ($\lambda = 0.2,\ \Lambda = 0°$, $C_{L_{mvr}}/C_L = 2.5$) with 10% untapered unswept winglets (Figure 19). There doesn't seem to be a significant advantage to changing the dihedral angle for this configuration other than in changing the location of the optimal span. Increasing dihedral toward vertical allows for decreased wing span as expected.

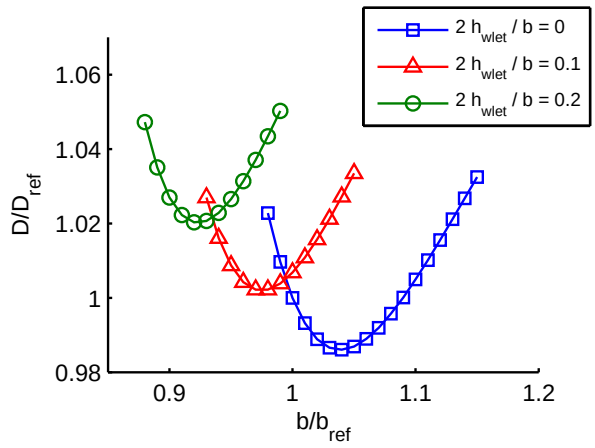

Figure 15. Variations in winglet height for an untapered wing ($C_{L_{mvr}}/C_L = 1$)

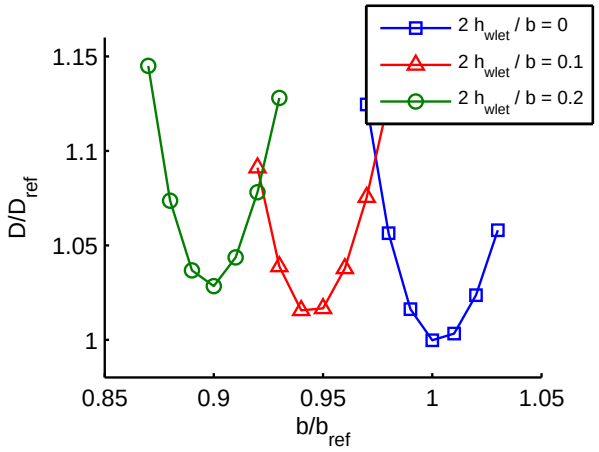

Figure 16. Variations in winglet height for an untapered wing ($C_{L_{mvr}}/C_L = 2.5$)

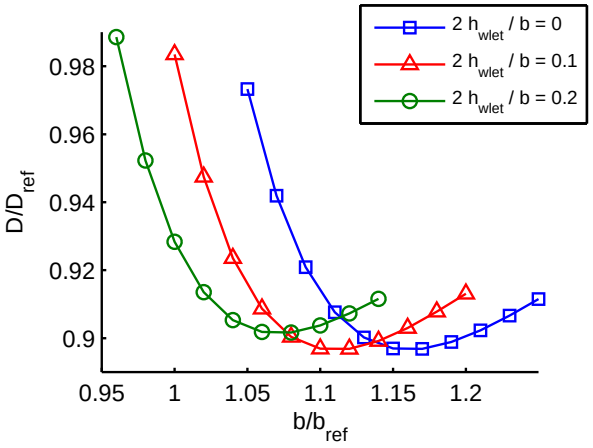

Figure 17. Variations in winglet height for a 0.2 taper ratio wing ($C_{L_{mvr}}/C_L = 1$)

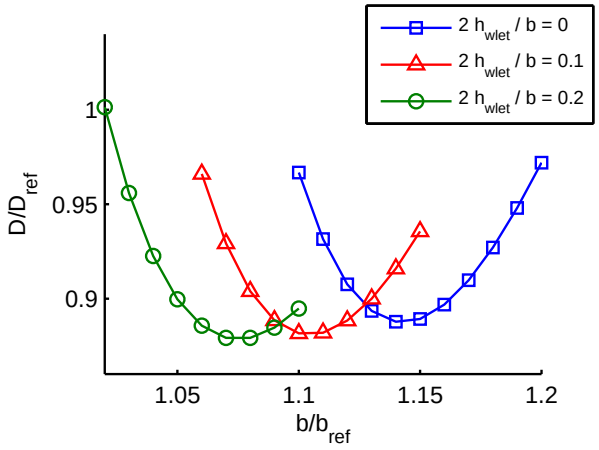

Figure 18. Variations in winglet height for a 0.2 taper ratio wing ($C_{L_{mvr}}/C_L = 2.5$)

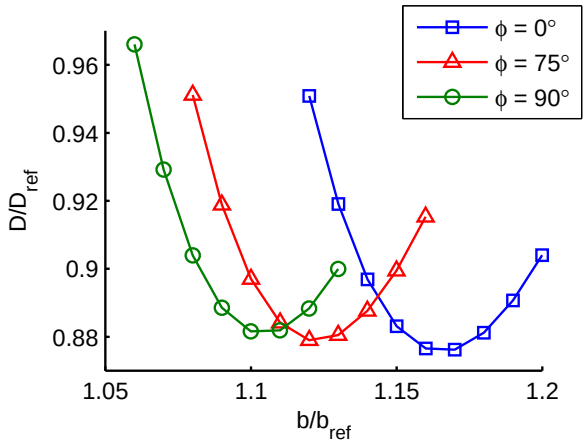

Figure 19. Variations in winglet dihedral angle for 0.2 taper ratio wing ($C_{L_{mvr}}/C_L = 2.5$)

3.6. Stall Speed Constraint

Before performing planform optimization, we consider a constraint on stall speed to limit unrealistically small tip chords. We have seen that small taper ratios are beneficial for drag reduction, but lead to high section lift coefficients and undesirable stall performance. Although viscous drag does increase with section c_l, the reduction in induced drag due to larger spans and smaller chords often offsets the penalty due to viscous drag, making this constraint necessary. As mentioned before, the optimization problem with these inequality constraints can be solved efficiently with convex programming.

For simplicity, we use a constant $c_{l_{max}}$ constraint across the wing. Typically, we would like to have a relatively flat c_l distribution at $C_{L_{max}}$. A perfectly flat c_l distribution would correspond to $c_{l_{max}}/C_{L_{max}} = 1.0$. This choice, however often makes the problem infeasible. A given c_l distribution and a given geometry uniquely determines the lift distribution, which does not necessarily satisfy the lift and weight constraints.

Figure 20 shows the effect of varying the ratio $c_{l_{max}}/C_{L_{max}}$. The wing analyzed is unswept and has a taper ratio of 0.2. Starting from the large values of $c_{l_{max}}$, where the constraint is inactive, we see that as we decrease $c_{l_{max}}$, initially there is no change in the minimum drag solution. As we start to approach $c_{l_{max}}/C_{L_{max}} = 1.0$ the optimal span increases and the drag starts to rise. If we set $C_{L_{mvr}}/C_L = 2.5$ we see a similar trend, however the drag penalty is a bit steeper (Figure 21).

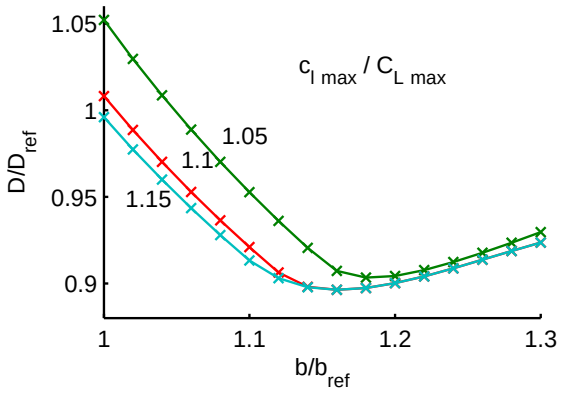

Figure 20. Effect of section c_l constraint for a 0.2 taper ratio wing ($C_{L_{mvr}}/C_L = 1.0$)

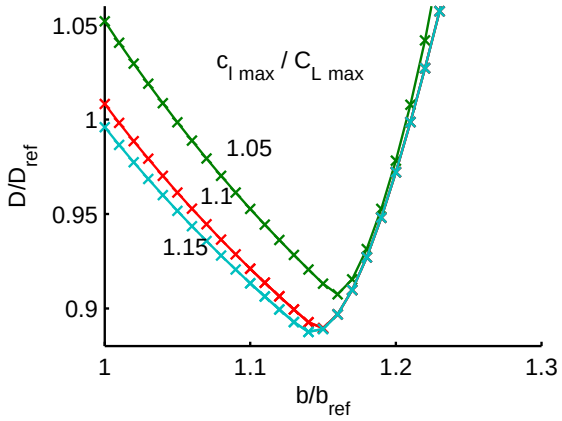

Figure 21. Effect of section c_l constraint for a 0.2 taper ratio wing ($C_{L_{mvr}}/C_L = 2.5$)

The variation of minimum drag solutions with $c_{l_{max}}/C_{L_{max}}$ is made more explicit in Figure 22. For large $c_{l_{max}}/C_{L_{max}}$ the solution is the same as the case when c_l was unconstrained. We would like to have a $c_{l_{max}}/C_{L_{max}}$ near 1 to force a relatively flat c_l distribution at $C_{L_{max}}$. We see that the flatter we make the c_l distribution, the greater the drag penalty. For example, at $c_{l_{max}}/C_{L_{max}} = 1.05$ there is a drag penalty of about 0.5% for $C_{L_{mvr}}/C_L = 1$ and a drag penalty of about 2% for $C_{L_{mvr}}/C_L = 2.5$ relative to the c_l unconstrained case.

Let us examine the c_l distribution to clarify some of the above discussion. The minimum drag loading from Figure 20 for the case $c_{l_{max}}/C_{L_{max}} = 1.05$ is shown in Figure 23. The constraint is active over a large portion of the wing, allowing a fairly flat c_l distribution.

The primary reason for including the stall speed constraint was so that planform optimization did not lead to unrealistically small chords. Let us now assess the effect on optimal taper ratio. Without the stall speed constraint, drag continues to decrease with decreasing taper ratio. Figures 24 and 25 show the minimum drag solutions (with respect to twist and span) as a function of taper ratio for a constraint of $c_{l_{max}}/C_{L_{max}} = 1.05$ and 1.2 respectively. The second constraint corresponds to $c_{l_{max}} = c_{l_{max}}|_{ref}$ for this case. The first constraint, leads to an optimum taper ratio that falls in a reasonable range (0.1 - 0.2). The second constraint does limit taper ratio but at rather small chords. This is due in part to the somewhat academic nature of this problem, in that twist is defined at every panel leading to a large number of degrees of freedom. In the following sections where the planform geometry is optimized, a more realistic representation of twist will be used and the constraint $c_{l_{max}} = c_{l_{max}}|_{ref}$ will suffice.

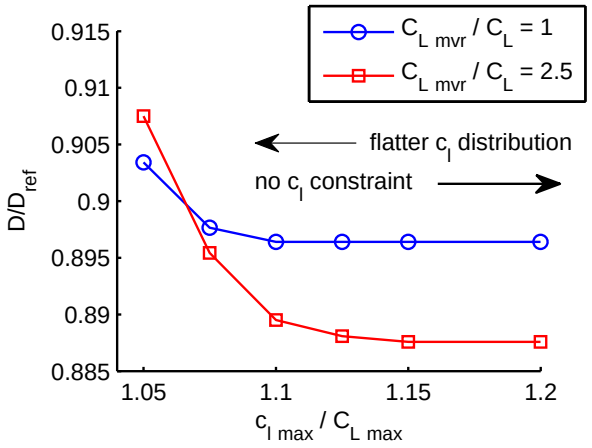

Figure 22. Drag rise with flatter c_l distribution

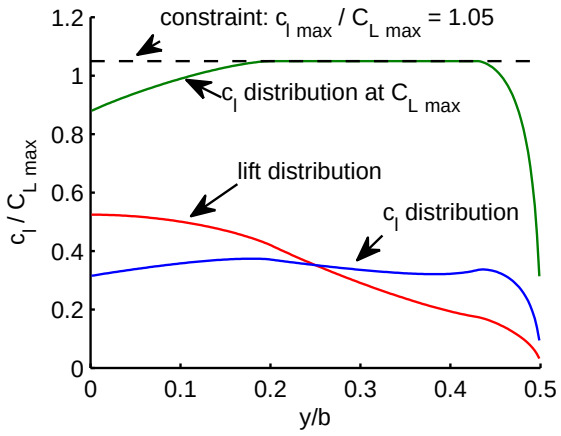

Figure 23. Optimal loading ($\lambda = 0.2, C_{L_{mvr}}/C_L = 1.0, c_{l_{max}}/C_{L_{max}} = 1.05$

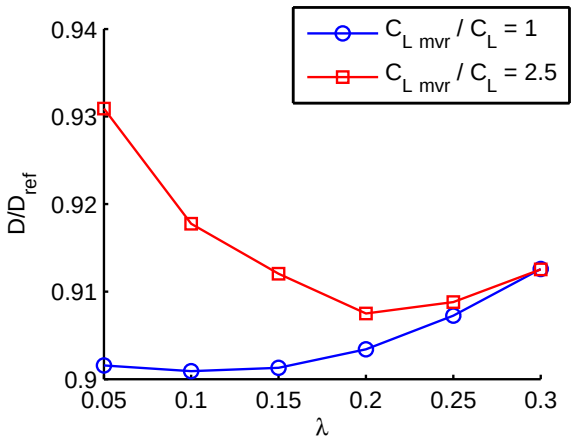

Figure 24. Minimum drag wings optimized for twist and span as a function of taper ratio ($c_{l_{max}}/C_{L_{max}} = 1.05$)

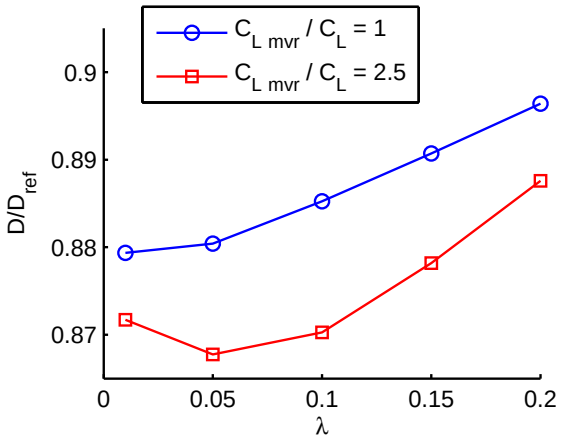

Figure 25. Minimum drag wings optimized for twist and span as a function of taper ratio ($c_{l_{max}}/C_{L_{max}} = 1.2$ or $c_{l_{max}} = c_{l_{max}}|_{ref}$)

4. Planform Optimization

Up to this point we have optimized the lift distribution for a given geometry. We took advantage of the resulting simple quadratic programming problem to rapidly perform trade studies. In the following sections we use nonlinear optimization to explore optimizing the planform geometry as well as the lift distribution.

4.1. Tip Extensions and Winglets - Retrofit

We start with the same baseline wing used by Whitcomb,[5] representative of early transport wings. The goal is to find the optimum tip geometry for this fixed wing planform. The geometry for the wing is seen in Figure 26, and the planform parameters are summarized in Table 1. Figure 26 also shows the tip extension tested by Whitcomb, whereas Figure 27 shows the winglet tested by Whitcomb.

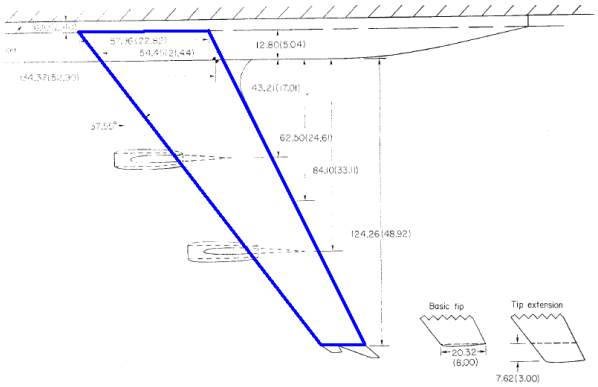

Figure 26. Geometry for baseline wing and Whitcomb tip extension

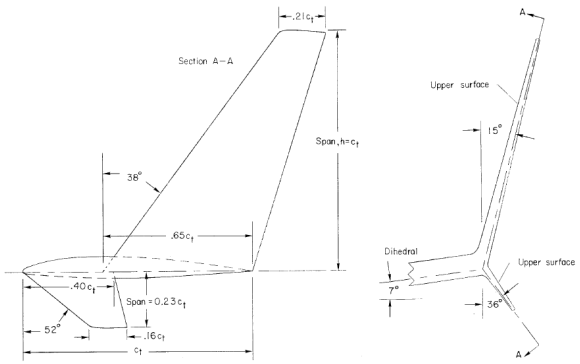

Figure 27. Winglet used by Whitcomb

Table 1. Baseline wing

AR	7
b	135 ft
Λ	35°
λ	0.35

Since we are only optimizing the tip geometry, we have a relatively small number of design variables. These include the length, root chord, tip chord, and quarter chord sweep of the tip geometry. Twist is also optimized across the wing and tip. Rather than letting the twist at every section be a design variable, as was done previously, we take a more realistic representation of twist. We define the twist at 3 sections across the wing, and 2 across the tip with a linear distribution of twist in between. The twist definition locations across the wing are at the root, 30% semi-span, and tip, whereas the twist locations for the tip geometry are at the root and tip. The dihedral angle of the tip geometry is fixed at different values to facilitate comparison between tip extensions and winglets.

The objective is to minimize total drag subject to constraints on lift, weight, and stall speed. Rather than constrain the wing to a particular weight, the target weight is varied in order to create a Pareto front of optimal solutions trading off drag and weight.

The optimization problem is posed as follows:

$$
\begin{aligned}
min \quad & J = \frac{D}{D_{ref}} \\
w.r.t. \quad & wing : \{\theta_{1,2,3}\},\ tip : \{\ell, c_r, c_t, \Lambda, \theta_{4,5}\} \\
s.t. \quad & 1 - \frac{L}{L_{ref}} \leq 0 \\
& \frac{W}{W_{target}} - 1 \leq 0 \\
& \{c_l\}|_{C_{L_{max}}} - \{c_{l_{max}}\} \leq 0
\end{aligned}
$$

$$
\begin{array}{ccccc}
0.01 & < & \frac{\ell}{b/2} & < & 0.65 \\
0.01 & < & \frac{c_r}{c_{t\,wing}} & < & 1 \\
0.01 & < & \frac{c_t}{c_{t\,wing}} & < & 1 \\
0^\circ & < & \Lambda & < & 40^\circ \\
-20^\circ & < & \theta_{1-5} & < & 20^\circ
\end{array}
$$

If sweep were allowed to vary freely, torsion-dependent weight and steady aeroelastics would need to be included. These have been explored in some computations, but for the present purposes they only complicate the problem formulation without providing much additional insight. Here, the tip sweep angle is not allowed to exceed 40°. The section maximum lift coefficient, c_{lmax}, is set equal to that of the reference wing.

There is one subtlety in the optimization procedure. The winglet length is a continuous design variable, but our analysis method is a discrete vortex panel method. For numerical accuracy the panel size across the wing and tip is constant. However, with a fixed panel size the number of panels on the tip will vary discontinuously. This is a problem for gradient based optimization, but is resolved by varying the tip length parametrically.

Figures 28 and 29 show the Pareto fronts at a C_{Lmvr}/C_L of 1 and 2.5 respectively. Also shown on these figures are a few of the optimized geometries to give a sense of relative size. The values shown in the figures denote the length of the tip normalized by the wing semi-span (i.e. for a tip extension a value of 0.14 corresponds to a 14% span increase).

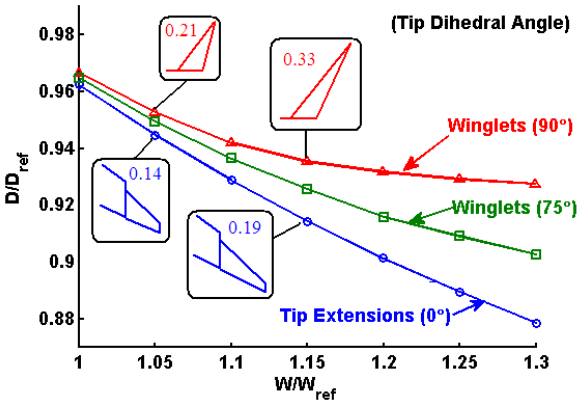

Figure 28. Pareto front of optimized tip extensions and winglets, relative size also shown ($C_{Lmvr}/C_L = 1.0$)

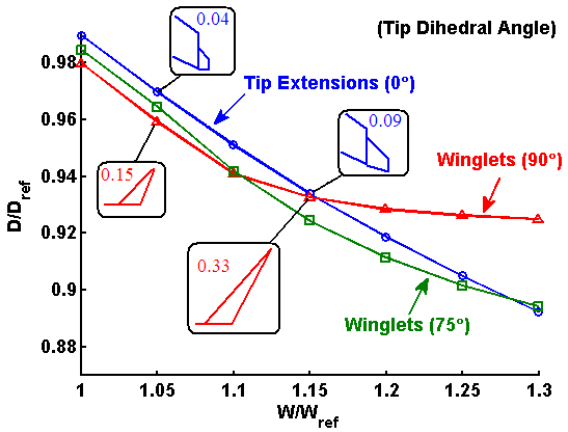

Figure 29. Pareto front of optimized tip extensions and winglets, relative size also shown ($C_{Lmvr}/C_L = 2.5$)

From these figures we see that for minimum drag the choice of tip extension versus winglet depends upon the ratio C_{Lmvr}/C_L. For $C_{Lmvr}/C_L = 1$ tip extensions outperform winglets for any weight increase. For a 5% weight increase the tip extension offers about a 1% reduction in drag relative to the optimized 90° winglet and about 0.5% relative to the 75° winglet.

However, for the case $C_{Lmvr}/C_L = 2.5$ winglets outperform tip extensions for all weights. A 90° winglet is optimal for weight increase less than 10% and a 75° winglet is optimal for larger weight increases. For a 5% weight increase the 90° winglet offers a 1% reduction in drag as compared to the tip extension.

Our computations are similar to the experimental results reported in Whitcomb's paper[5] if we use the same criteria. For example, we predict that the Whitcomb winglet offers about a 7% increase in L/D as compared to the reported 9%, and the Whitcomb tip extension offers a 4% increase in L/D as compared to the reported 4% (These values are at the same increase in root bending moment reported in the paper of about 3.5%).

However, the results are quite different when using integrated bending moment over thickness rather than root bending moment for weight, and when including stall constraints. The chords on the winglet are smaller than those on the tip extensions, leading to a small penalty at C_{Lmax}. Figures 30 and 31 show the same Pareto fronts, but include the calculations based on Whitcomb's actual tip extension/winglet geometry with optimized twist across the wing and tip. Two sets of points are shown, one set with no constraint on

weight, and one set constrained to less than 5% weight increase. In both cases the Whitcomb winglet is far closer to an optimum design than the Whitcomb tip extension.

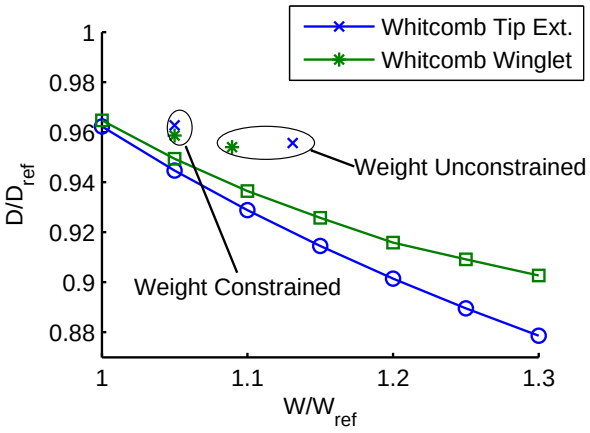

Figure 30. Whitcomb winglet shown to be much closer to an optimal design than Whitcomb tip extension ($C_{L_{mvr}}/C_L = 1.0$)

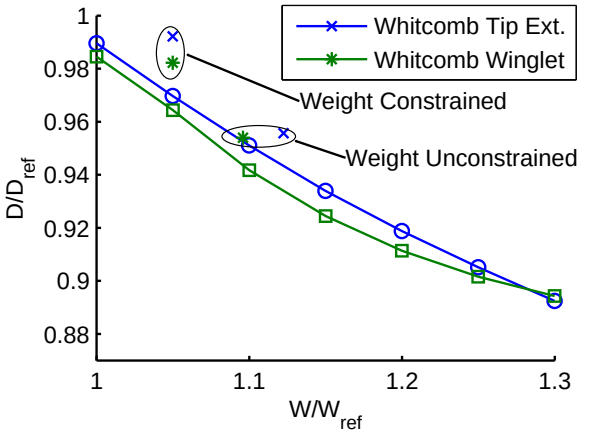

Figure 31. Whitcomb winglet shown to be much closer to an optimal design than Whitcomb tip extension ($C_{L_{mvr}}/C_L = 2.5$)

Although we have seen that for minimum drag the choice of tip extensions versus winglet depends on the ratio $C_{L_{mvr}}/C_L$, the difference in drag is small. The choice of whether to use a tip extensions or a winglet would more likely be determined by other considerations such as stability and control, lateral dynamics, structural dynamics, or even marketing.

4.2. Tip Extensions and Winglets - New Wing Design

We now examine a more general wing design problem by allowing the entire planform shape to vary. Rather than using a trapezoidal wing and a trapezoidal tip, we employ a more general description of the geometry by using a larger number of trapezoidal sections. Five trapezoidal sections are used equally spaced across the wing, and the tip is one separate trapezoidal section. The following design variables were used: wing span, tip length, chord length at each section, twist at each section, and dihedral angle of the tip. As done before, the length of the wing and the length of the tip are varied parametrically. Since transonic drag rise and torsional weight are not included in the computation, the sweep of the wing is fixed at the value of the reference wing. As demonstrated previously, the sensitivity of drag to the tip dihedral angle is often very small, thus care must be taken to scale this variable properly in order to get correct solutions.

The constraints include minimum lift, maximum weight, and minimum stall speed. In addition we include a constraint that the lift distribution at maneuver is positive at every section. A negative maneuver loading can produce negative weight for some sections if not handled properly. For these problems negative loading is almost never optimal, but if not constrained can be exploited by the optimizer. This will be explored in more detail later for cases where negative loading may be optimal.

The optimization problem is given as:

$$
\begin{aligned}
min \quad & J = \frac{D}{D_{ref}} \\
w.r.t. \quad & b, \ell_{tip}, \{c\}, \{\theta\}, \phi_{tip} \\
s.t. \quad & 1 - \frac{L}{L_{ref}} \leq 0 \\
& \frac{W}{W_{ref}} - 1 \leq 0 \\
& \{c_l\}|_{C_{L\,max}} - \{c_{l\,max}\} \leq 0 \\
& -\frac{\{\gamma_{mvr}\}}{\overline{\gamma}_{ref}} \leq 0
\end{aligned}
$$

$$
\begin{array}{ccccc}
0.5 & < & \frac{b}{b_{ref}} & < & 2 \\
0.01 & < & \frac{\ell_{tip}}{b_{ref}} & < & 0.5 \\
0.01 & < & \frac{c}{c_{ref}} & < & 5 \\
-20^\circ & < & \theta & < & 20^\circ \\
\frac{0^\circ}{1000} & < & \frac{\phi_{tip}}{1000} & < & \frac{120^\circ}{1000}
\end{array}
$$

The reference wing used in this computation (and in the next few sections) is a more modern wing shape than used in the Whitcomb study. The definitions for aspect ratio, taper ratio, and root chord used in the figure to the right are based upon the trapezoidal reference area only. The span of the reference wing is 200 ft.

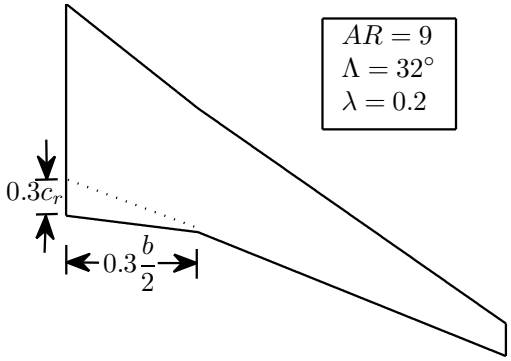

The optimized planform shape is shown for a $C_{Lmvr}/C_L = 1$ and 2.5 in Figures 32 and 33 respectively. The optimal tip designs depend on C_{Lmvr}/C_L in a similar manner to the tip geometries from the last section. For a $C_{Lmvr}/C_L = 1$ the optimal design uses a tip extension and achieves a drag reduction of about 6% relative to the baseline wing. The span has increased by 6% of the reference wing span. At $C_{Lmvr}/C_L = 2.5$ the optimal design uses a 85° dihedral winglet and achieves a drag reduction of about 4%. The wing span is 94% of the reference wing span, and the winglet length is 20% of the wing semi-span. Again, differences between the winglet designs and tip extensions designs are small in terms of lift to drag ratios.

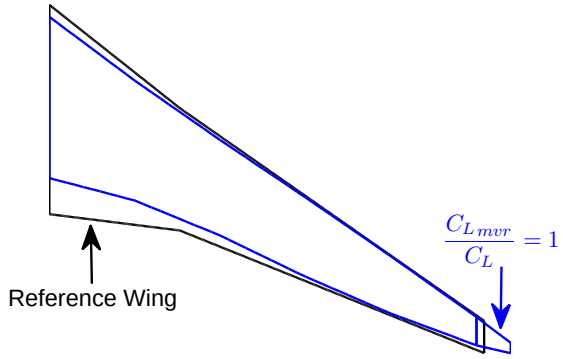

Figure 32. Optimized planform and tip - 0° dihedral ($C_{Lmvr}/C_L = 1.0$)

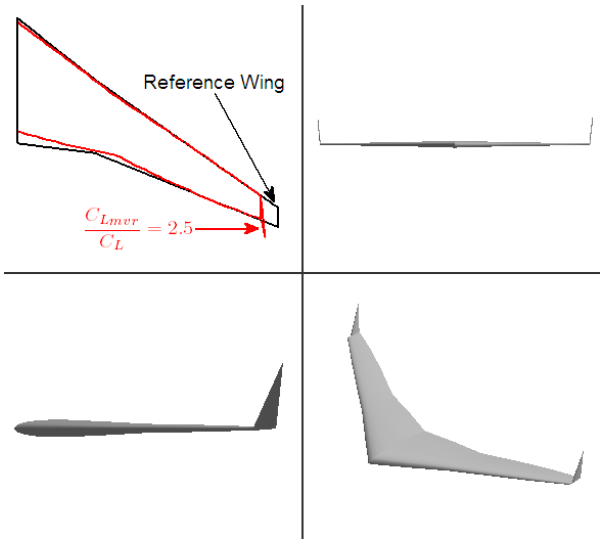

Figure 33. Optimized planform and tip - 85° dihedral ($C_{Lmvr}/C_L = 2.5$)

4.3. C-Wings for Tailless Aircraft

In the previous planform optimization problems, we did some studies with C-wings but never found any significant benefit as compared to a wing with a winglet. For a tailless aircraft however, a C-wing could be beneficial for its effect on the pitching moment about the aerodynamic center. The current method can be used to include constraints on pitching moment.

4.3.1. Additional Constraints

A few modifications must be made to the constraints to properly handle C-wings. The first change is that the local circulation must be allowed to be either positive or negative. In previous cases we always constrained the loading to be positive across the wing at the maneuver load. Allowing the loading to be negative introduces changes to the weight computation, the stall speed constraint, and the skin thickness constraint (mentioned below).

The computation of the bending weight must be slightly modified for cases where the loading may be negative at some sections (more detail is provided in the Appendix). This is because the volume of material used to resist bending loads actually depends on the absolute value of the local bending moment. The implementation of the weight constraints must also be modified accordingly as outlined below.

Weight is given by:

$$W = \left|\left|\left\{\frac{M_b}{t}ds\right\}\right|\right|_1 + k_W S$$

where the sum is taken across a semi-span. The 1-norm cannot be used directly as a constraint for gradient-based optimization. Incorporating a 1-norm constraint requires that we consider all possibilities of the summation as constraints. Generally, this would require 2^N constraints where N is the number of elements in the sum (in this case N would be the number of panels). This can lead to a very large number of constraints. However, we can use our knowledge of what a typical M_b/t distribution looks like (see figure to the right) to reduce the number of constraints. First, we notice that over most of the wing the local bending moment will be positive. However, at the tip of the wing, and on the tip devices, the bending moment may be negative. Therefore, we can break up the sum into a component over the inner part of the wing, which can be computed in the same manner as before, and a sum over the tip.

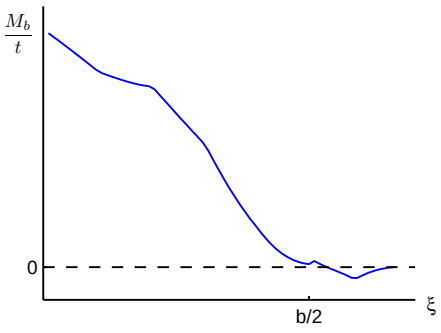

$$W = I_{binner} + \left|\left|\left\{\frac{M_b}{t}ds\right\}\right|\right|_{1outer} + k_W S$$

We further notice that typically the sign of the local bending moment will change only once (although we must check afterward that this is indeed the case). This reduces the number of possible summations to scale linearly with P, where P is the number of panels over the outer portion of the wing. We can define this vector of possible summations by multiplying the bending moment over thickness distribution times a matrix of ones whose upper diagonal is negative.

$$\{I_b\}_{outer} = \begin{bmatrix} 1 & -1 & -1 & -1 & -1 \\ 1 & \ddots & -1 & -1 & -1 \\ 1 & 1 & \ddots & -1 & -1 \\ 1 & 1 & 1 & \ddots & -1 \\ 1 & 1 & 1 & 1 & 1 \end{bmatrix} \begin{bmatrix} \left(\frac{M_b}{t}ds\right)_1 \\ \left(\frac{M_b}{t}ds\right)_2 \\ \left(\frac{M_b}{t}ds\right)_3 \\ \left(\frac{M_b}{t}ds\right)_4 \\ \vdots \\ \left(\frac{M_b}{t}ds\right)_P \end{bmatrix}_{outer}$$

The P constraints can now be posed as

$$I_{binner} + \{I_b\}_{outer} + k_W S \leq W_{ref}$$

Negative loading also requires that we add additional constraints related to the stall speed. C_{Lmax} is computed in the same manner, however we now require that

$$\{|c_l|\}|_{C_{Lmax}} \leq \{c_{lmax}\}$$

The constraint can be handled in the same way over the inner portion of the wing, however over the outer portion of the wing we must use additional constraints of the form:

$$\{c_l\}|_{C_{Lmax}} \leq \{c_{lmax}\}$$

and

$$\{c_l\}|_{C_{L\,max}} \geq -\{c_{l\,max}\}$$

The second modification required for C-wing optimization is related to the skin thickness. The optimizer would like to unload the winglet, and drive the winglet to very small chords to reduce drag and weight. But to support the C-wing element this would require very large skin thicknesses in the winglet. The structural model assumes that the skin thickness is much smaller than the airfoil thickness. We must place a constraint on the skin thickness of the structural box to prevent unreasonable designs. For the wing structural box the bending moment is given as

$$M_b = \sigma \frac{t}{2} A$$

where σ is the yield stress (assuming a fully stressed wing at the limit load), t is the airfoil thickness, and A is the total cross sectional area of the stressed material. The cross-sectional area of the stressed material can be approximated by $A = 2t_s c_b$ where t_s is the skin thickness and c_b is the chord length of the structural box. We can now compute the skin thickness as

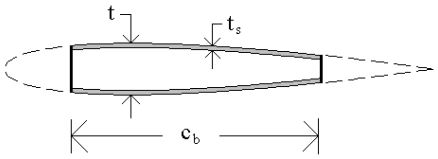

$$t_s = \left(\frac{M_b}{t}\right) \frac{1}{\sigma\ c_b}$$

We are already computing $\frac{M_b}{t}$ at every section, and typically c_b is about 60% of the local chord. For the yield stress we use 54,000 psi, which is a typical value for design stress at limit load. We now constrain the local skin thickness to be smaller than 10% of the local airfoil thickness.

Allowing negative bending moments over the outer portion of the wing increases the number of skin thickness constraints needed. The skin thickness is actually proportional to the absolute value of the local bending moment. Similar to the constraint on $c_{l\,max}$, we just need to add additional constraints on the outer portion of the wing of the form:

$$\begin{aligned} \{t_s\} &\leq 0.1t \\ \{t_s\} &\geq -0.1t \end{aligned}$$

One final modification is necessary in optimizing C-wings. Instead of specifying one critical maneuver C_L at a time, as we have been doing, we compute the weight at multiple maneuver lift coefficients and take the weight to be the maximum of those computed at the various conditions. The C-wing element effectively acts like a tail, making this consideration important. If only one $C_{L\,mvr}$ is examined the C-wing element can unload at the maneuver C_L so that it seemingly adds very little structural weight while still providing the benefit in pitching moment about the aerodynamic center. All this means is that we haven't really examined the critical maneuver C_L. Instead, the weight is evaluated at cruise C_L and at 2.5 times the cruise C_L and the weight is taken to be maximum of the two conditions. Considering intermediate values of C_L is not necessary since the additional load distribution changes monotonically between the two tested conditions. Again, additional constraints must be added since max cannot be used directly in the optimization. We require $W|_{C_{L_1}} < W_{ref}$ and $W|_{C_{L_2}} < W_{ref}$. Since the skin thickness depends on the maneuver bending moment distribution, the number of skin thickness constraints must also be doubled.

4.3.2. Weight-Constrained Designs

For the optimization problem the wing is divided into five trapezoidal sections, one vertical winglet, and one horizontal C-wing element. The design variables include the wing span, the chord lengths at each section, and the twist at each section. Since the length of each lifting surface must be varied parametrically the number of combinations can become large. Rather than exhaustively explore this design space, we specify a fixed winglet height and fixed C-wing element length of 16% of the wing semi-span. The sweep of the main wing is fixed at 32° and the sweep of the winglet and C-wing element are both fixed at 20°. The optimization problem is given as follows:

$$
\begin{aligned}
min \quad & J = \frac{D}{D_{ref}} \\
w.r.t. \quad & b, \{c\}, \{\theta\} \\
s.t. \quad & 1 - \frac{L}{L_{ref}} \leq 0 \\
& \frac{(I_{binner} + \{I_b\}_{outer} + k_W S)_{C_{L1}}}{W_{ref}} - 1 \leq 0 \\
& \frac{(I_{binner} + \{I_b\}_{outer} + k_W S)_{C_{L2}}}{W_{ref}} - 1 \leq 0 \\
& \{c_l\}|_{C_{L\,max}} - \{c_{l\,max}\} \leq 0 \\
& -\{c_l\}|_{C_{L\,max}} - \{c_{l\,max}\} \leq 0 \\
& 10(\{t_s\}|_{C_{L1}} - 0.1\{t\}) \leq 0 \\
& 10(\{t_s\}|_{C_{L2}} - 0.1\{t\}) \leq 0 \\
& 10(-\{t_s\}_{outer}|_{C_{L1}} - 0.1\{t\}) \leq 0 \\
& 10(-\{t_s\}_{outer}|_{C_{L2}} - 0.1\{t\}) \leq 0 \\
& C_{mac} - C_{mac\ target} = 0
\end{aligned}
$$

$$
\begin{array}{ccccc}
0.5 & < & \frac{b}{b_{ref}} & < & 5 \\
0.01 & < & \frac{c}{c_{ref}} & < & 5 \\
-20^\circ & < & \theta & < & 20^\circ
\end{array}
$$

Three different constraints on pitching moment about the aerodynamic center are explored: $C_{mac\ target} = +0.1, 0, -0.1$. For each target, the optimal C-wing is compared to an optimized wing with winglet and an optimized wing subject to the same constraints. The minimum drag solution for each configuration is shown in Table 2 normalized by the drag of the reference wing. Table 3 lists the optimized span of each configuration normalized by the span of the reference wing. The sign convention used in the following figures as well as the definition of the coordinate ξ is show in Figure 34.

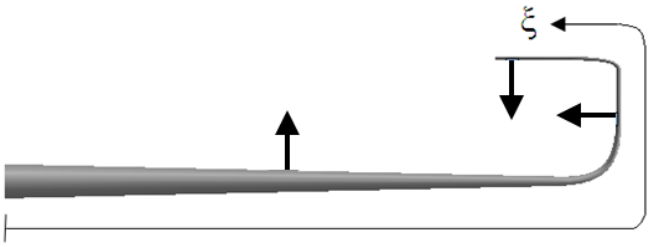

Figure 34. Sign convention for positive loading

Table 2. Relative drag (D/D_{ref}) of optimized configurations - weight constrained

C_{mac}	Wing	Wing + Winglet	C-wing
+0.1	1.091	1.095	**1.081**
0	0.978	**0.964**	0.971
-0.1	1.345	**1.316**	1.321

For $C_{mac} = +0.1$ the optimal design is the C-wing. It has about 1% less drag, and a 9% smaller span relative to the optimized wing. The geometry for the optimized wing and the optimized C-wing is shown in Figures 35 and 36. The winglet and C-wing element have small chords, requiring additional assessment of structural dynamics. The lift distributions for these two cases are shown in Figures 37 and 38. The lift distribution is plotted as a function of the coordinate ξ, which traverses the surface of the wing. In both

Table 3. Relative spans (b/b_{ref}) of optimized configurations - weight constrained

C_{mac}	Wing	Wing + Winglet	C-wing
+0.1	1.078	1.076	0.977
0	1.00	0.956	0.947
-0.1	0.959	0.907	0.902

cases the pitching moment constraint is met by shifting the load far inboard. The C-wing element does provide some nose-up pitching moment. The wing design has a large span, but is actually downloaded at the tip to help meet the pitching moment constraint.

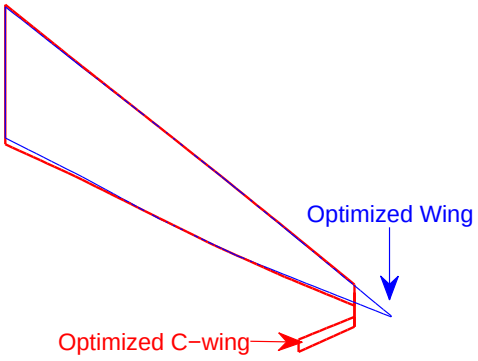

Figure 35. Optimized wing and C-wing top view ($C_{mac} = +0.1$)

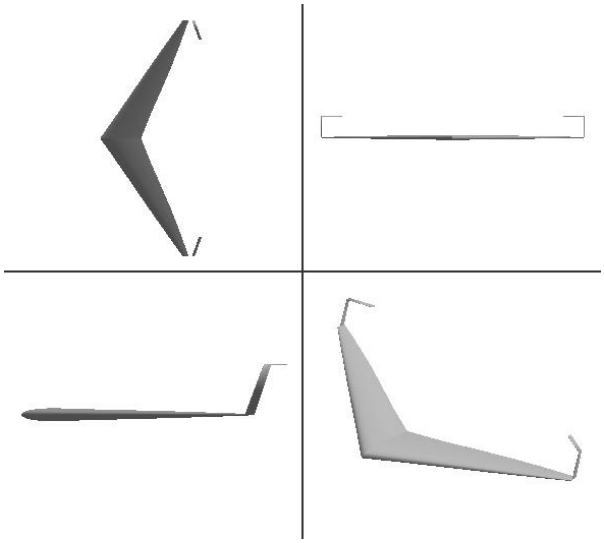

Figure 36. Optimized C-wing ($C_{mac} = +0.1$)

For the constraint $C_{mac} = 0$ the optimal design is a wing with a winglet. The optimal wing with winglet reduces the drag by about 1.5% and has a 5% smaller span relative to the optimized wing. The optimal wing and the optimal wing with winglet are seen in Figures 39 and 40. The lift distribution for the configurations are seen Figures 41 and 42. The lift distribution is nearly elliptic for both cases.

For $C_{mac} = -0.1$ the optimal design is also a wing with a winglet. The optimal geometry is seen in Figures 43 and 44. The wing with winglet design achieves a drag reduction of 2%, and has a 5% smaller span relative to the optimized wing. The lift distribution for the two configurations are seen in Figures 45 and 46. In both cases the lift distribution is heavily shifted outboard to satisfy the pitching moment constraint. These wings have rather large chords inboard to carry the bending weight. The large changes in chord makes some of our assumptions suspect. Three-dimensional viscous drag effects make the section viscous drag buildup method less accurate. Also the large chord variation makes the assumption of a constant t/c a worse approximation. Further analyses would be required for these designs to more completely assess their relative benefits.

In all three cases, however, the difference in drag between the wing, wing with winglet, and C-wing never differs by more than a percent or two. Likely the configuration choice would be dictated by something other than drag such as span, structural dynamics, or radar cross section.

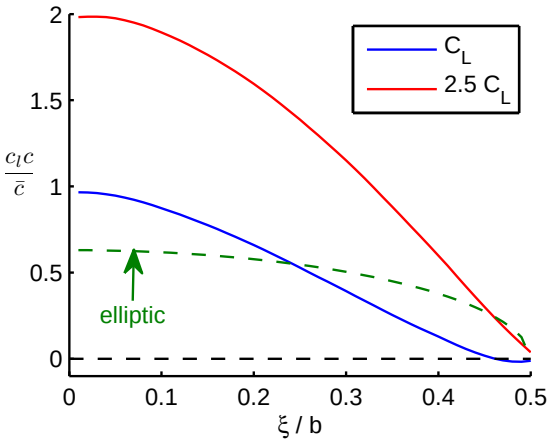

Figure 37. Wing lift distribution ($C_{m_{ac}} = +0.1$)

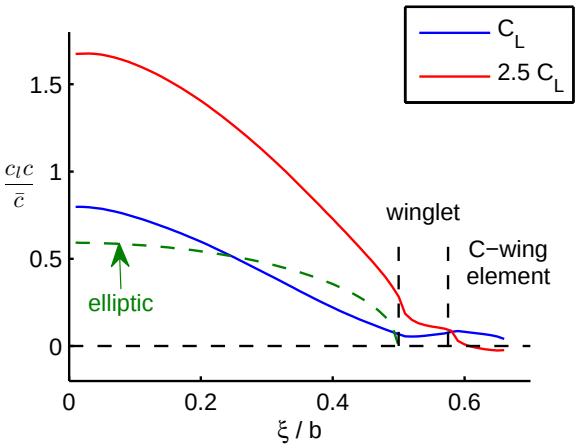

Figure 38. C-wing lift distribution ($C_{m_{ac}} = +0.1$)

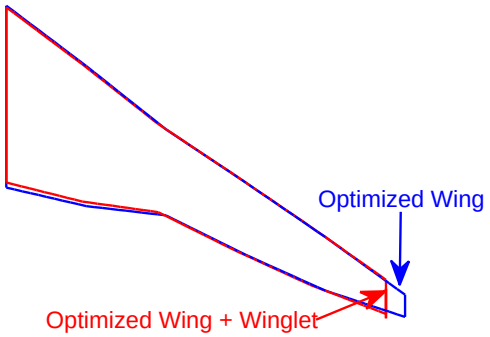

Figure 39. Optimized wing and wing with winglet ($C_{m_{ac}} = 0$)

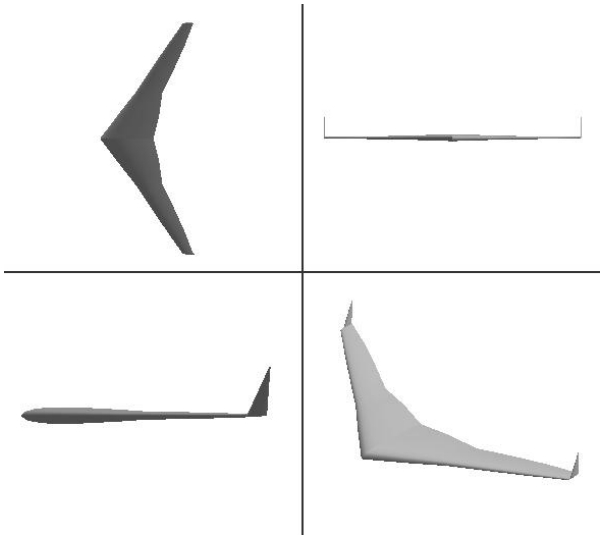

Figure 40. Optimized wing with winglet ($C_{m_{ac}} = 0$)

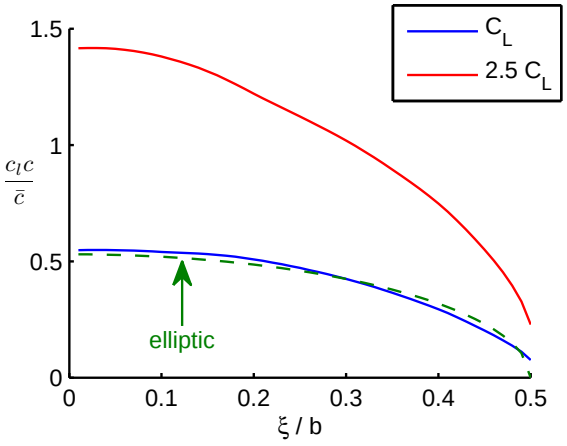

Figure 41. Wing lift distribution ($C_{m_{ac}} = 0$)

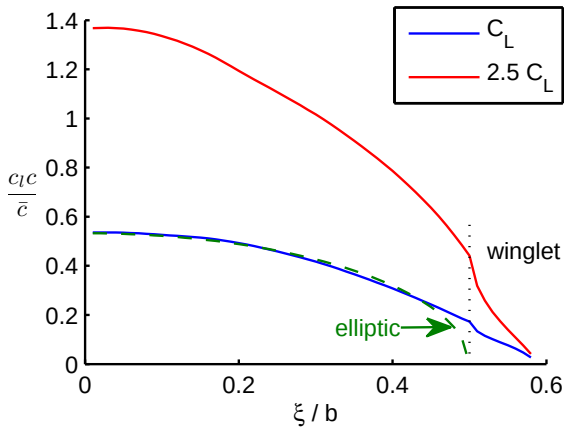

Figure 42. Wing with winglet lift distribution ($C_{m_{ac}} = 0$)

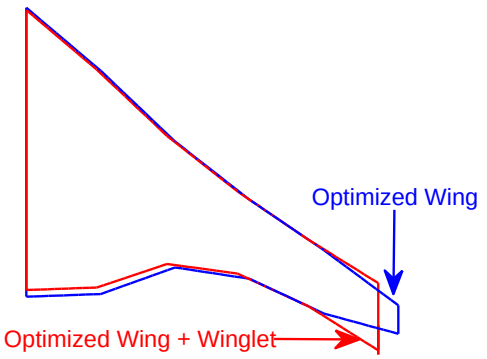

Figure 43. Optimized wing and wing with winglet ($C_{m_{ac}} = -0.1$)

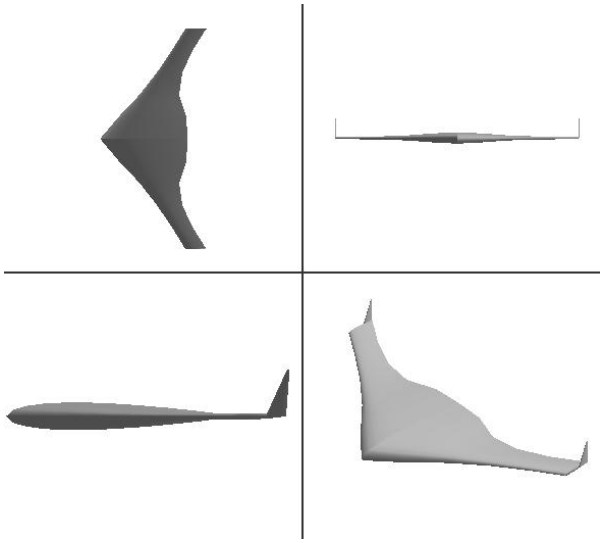

Figure 44. Optimized wing with winglet ($C_{m_{ac}} = -0.1$)

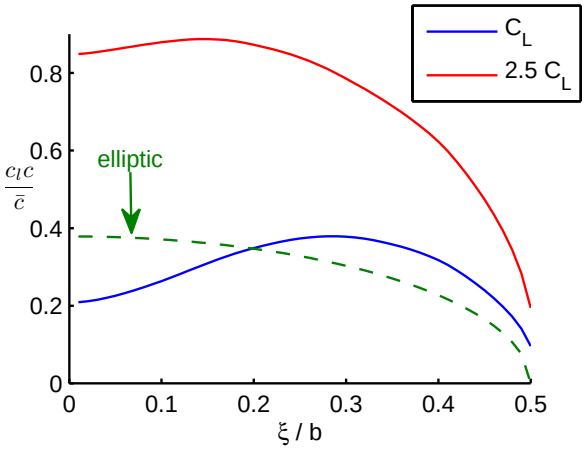

Figure 45. Wing lift distribution ($C_{m_{ac}} = -0.1$)

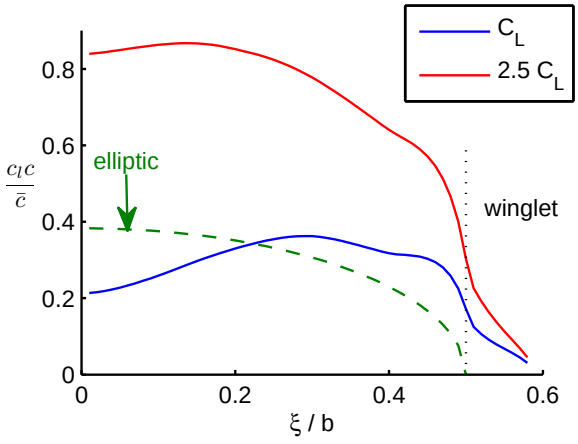

Figure 46. C-wing lift distribution ($C_{m_{ac}} = -0.1$)

4.3.3. Span-Constrained Designs

Let us now consider the effect of span constraints on C-wing designs. We saw that the variation in drag was small between the different configurations at a given pitching moment constraint, however the variation in span was much larger. We know that winglets can improve designs with span constraints, but it is not clear if C-wings add any additional benefit for span-constrained wings. We compare optimized wings, wings with winglets, and C-wings, all constrained to have a span less than or equal to that of the reference wing. Rather than fix the weight at a particular value, the results are presented as a Pareto front. As mentioned before, the winglet height and C-wing element length are fixed at 16% of the wing semi-span.

The results are shown in Figures 47 - 52. For each pitching moment constraint the Pareto front is shown along with the optimal design at a weight increase of 30% above the reference wing. In most cases the majority of the drag reduction is achieved at around a 30% weight increase.

From the figures we see that at a pitching moment constraint of $C_{mac} = +0.1$, C-wings do provide significant drag reductions as opposed to wings with winglets. The C-wing has 3% less drag than the wing with winglet, and 5% less drag than the wing at $W/W_{ref} = 1.3$. At a C_{mac} of 0 and -0.1 there is no aerodynamic benefit to C-wings as compared to wings with winglets. At a C_{mac} of 0 the wing with winglet has 0.5% less drag than the optimized C-wing, and 5% less drag than the optimized wing at $W/W_{ref} = 1.3$. At a C_{mac} of -0.1 the wing with winglet has 0.5% less drag than the optimized C-wing, and 7% less drag than the optimized wing at $W/W_{ref} = 1.3$.

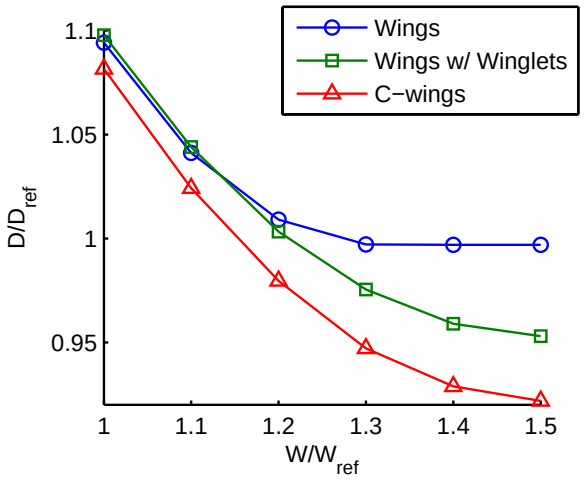

Figure 47. Pareto front for optimized span constrained designs ($C_{mac} = 0.1$)

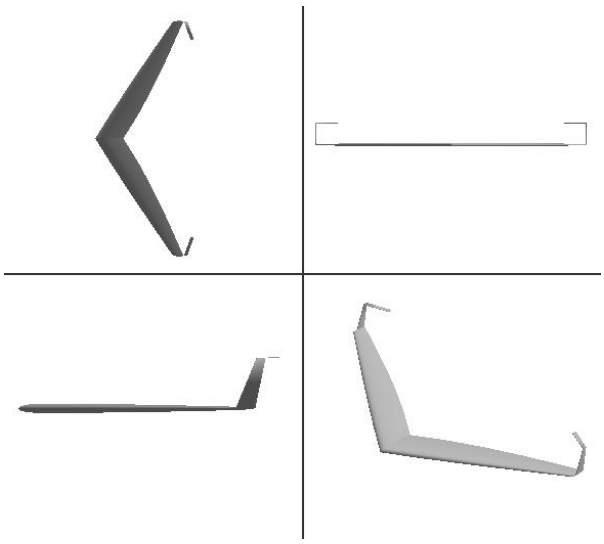

Figure 48. Optimized C-wing ($C_{mac} = 0.1$ **and** $W/W_{ref} = 1.3$)

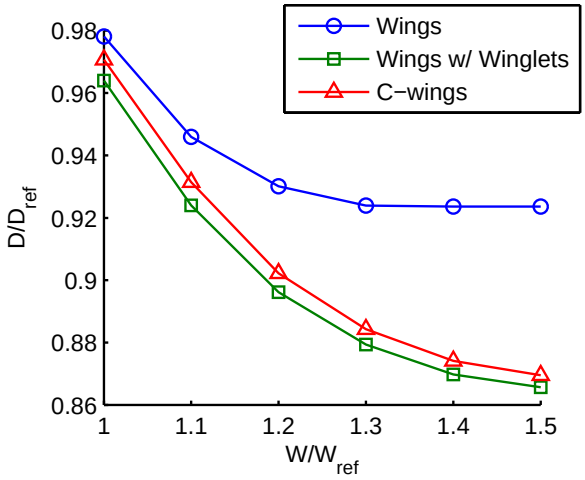

Figure 49. Pareto front for optimized span constrained designs ($C_{m_{ac}} = 0$)

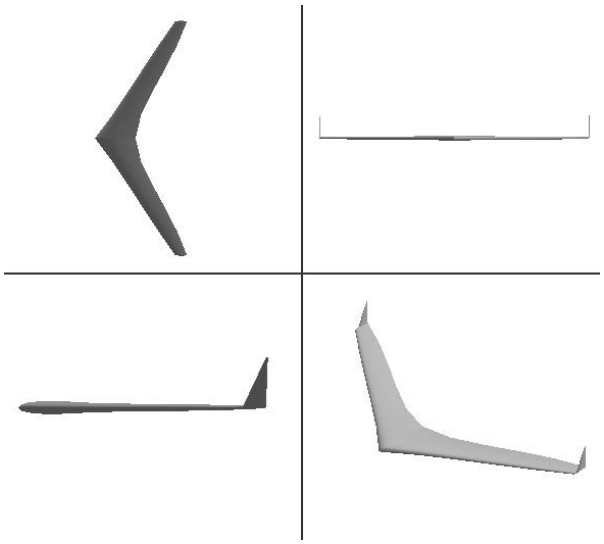

Figure 50. Optimized wing with winglet ($C_{m_{ac}} = 0$ and $W/W_{ref} = 1.3$)

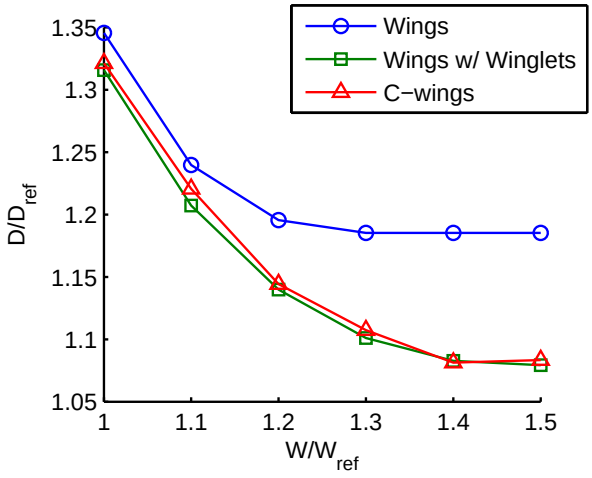

Figure 51. Pareto front for optimized span constrained designs ($C_{m_{ac}} = -0.1$)

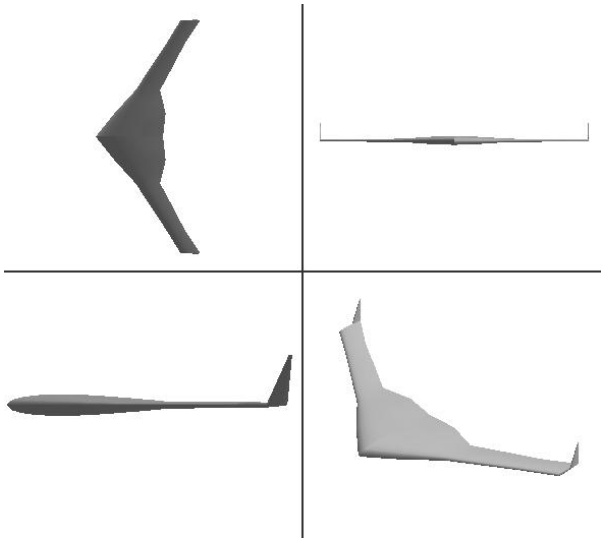

Figure 52. Optimized wing with winglet ($C_{m_{ac}} = -0.1$ and $W/W_{ref} = 1.3$)

4.3.4. Effect of Sweep on C-wing Designs

The results discussed so far have been for a relatively highly swept wing (32° quarter chord sweep) to account for transonic effects. However, lately there has been much interest in returning to low sweep wings for the benefits of natural laminar flow. Through careful aerodynamic shape optimization, low sweep wings can be designed to avoid premature transonic drag rise. Changing the sweep of the main wing can have a more dramatic effect on C-wing designs. We have seen that C-wings provide some benefit relative to wing and wing with winglet designs for positive pitching moment requirements. At low sweep angles, wing designs must employ even greater washout to provide nose up pitching moment while C-wing designs can increase the loading on the C-wing element to provide nose up pitching moments without the need for as much washout. Thus, we expect the benefits of C-wings may be greater for low sweep designs. The effect of changing the main wing sweep is quantified in Figure 53. In this study the height of the winglet and length of the C-wing element were still fixed, however they were fixed at a larger value than the previous results. For low sweep designs, the optimizer would like to have larger winglets and C-wing elements to provide the nose up pitching moment. Increasing the size of the winglet and C-wing element has only a small benefit at the higher sweep angles examined previously. The results shown here are for a winglet height and C-wing element length of 25% of the semi-span. This length, while not precisely optimal, was found to achieve most of the benefit in drag without being unnecessarily large. For a main wing sweep of 20° the C-wing design show roughly an 8% drag reduction as compared to the optimized wing design. The C-wing design with 20° sweep is shown in Figure 54. We can see with a fixed quarter chord sweep, and the winglet aligned with the trailing edge of the wing tip, the optimizer would like to increase the tip chord so as to move the winglet and C-wing element further aft. This allows a greater moment arm for the pitching moment. The decrease in necessary washout compensates for the decrease in span due to larger tip chords.

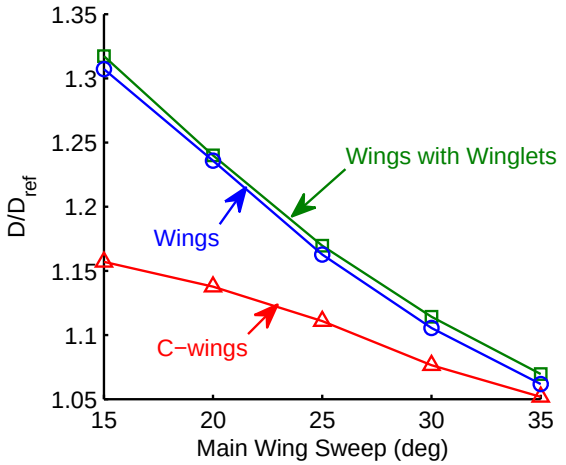

Figure 53. Effect of changing the main wing sweep ($C_{m_{ac}} = +0.1$)

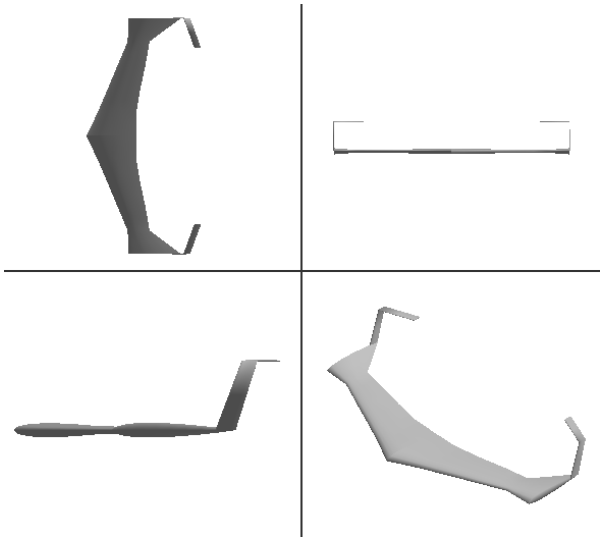

Figure 54. Optimized C-wing ($C_{m_{ac}} = +0.1$ **and** $\Lambda = 20°$)

4.4. Maneuver Load Alleviation

The method described here can also be applied to wings with active load alleviation. In many of the previous computations we have seen how the optimal design depends upon the ratio C_{Lmvr}/C_L. For a C_{Lmvr}/C_L other than 1 we have noticed that the additional lift distribution may be tailored to simultaneously allow an efficient cruise load and an inboard loaded maneuver load. If we are also able to change the basic lift distribution (i.e. dynamically twist the wing), then we can exploit the difference between an ideal cruise load distribution and an ideal structural limit load distribution even further. Here, we assume that the aircraft can provide gust load alleviation in a similar manner, but that the structure is critical at maneuver.

For simplicity, we consider a planar wing with five trapezoidal sections and no tip devices. The design variables include span, chord at each section, and twist at each section. We now add to our design variables the twist distribution at the maneuver load. The cruise loading and structural limit loading are then only coupled through the planform geometry, whereas without maneuver load alleviation they are also coupled

through the twist distribution. The objective is to minimize drag at cruise subject to constraints on cruise lift, maneuver lift, maneuver weight, and stall speed. Additionally the maneuver lift distribution must not exceed $c_{l_{max}}$ at any section. Since we are examining a planar wing, we also fix the wetted area allowing us to use bending weight only. The optimization problem is given as:

$$
\begin{aligned}
min \quad & J = \frac{D}{D_{ref}} \\
w.r.t. \quad & b, \{c\}, \{\theta\}, \{\theta\}_{mvr} \\
s.t. \quad & 1 - \frac{L}{L_{ref}} \leq 0 \\
& 1 - \frac{L_{mvr}}{2.5\ L_{ref}} \leq 0 \\
& \frac{W_{mvr}}{W_{ref}} - 1 \leq 0 \\
& \{c_l\}|_{C_{L_{max}}} - \{c_{l_{max}}\} \leq 0 \\
& \{c_l\}|_{C_{L_{mvr}}} - \{c_{l_{max}}\} \leq 0 \\
& -\frac{\{\gamma_{mvr}\}}{\overline{\gamma}_{ref}} \leq 0 \\
& \frac{S}{S_{ref}} - 1 = 0
\end{aligned}
$$

$$
\begin{array}{ccccc}
0.5 & < & \frac{b}{b_{ref}} & < & 5 \\
0.01 & < & \frac{c}{c_{ref}} & < & 5 \\
-20^\circ & < & \theta & < & 20^\circ \\
-20^\circ & < & \theta_{mvr} & < & 20^\circ
\end{array}
$$

Since the twist distribution at maneuver is independent of the twist distribution at cruise, the parameter C_{Lmvr}/C_L is no longer important. Instead the parameter $c_{l_{max}}/C_{Lmvr}$ governs the design. This parameter reflects the degree to which the maneuver lift distribution is constrained by stall, similar to the simple analysis showing the effect of the stall speed constraint (Section 3.6). This ratio approaches one (flatter c_l distribution) as the critical structural altitude is increased, or as the cruise lift coefficient is increased at fixed altitudes.

The reduction in drag from using maneuver load alleviation (MLA) is shown in Figure 55. As we increase $c_{l_{max}}/C_{Lmvr}$ even greater drag reductions are possible. However, designs with maneuver load alleviation tend toward very large aspect ratios. In this case, flutter becomes an important consideration not accounted for here. Thus, in this paper, we limit our attention to cases where $c_{l_{max}}/C_{Lmvr}$ is close to one. For these cases, using maneuver load alleviation offers about 15-20% drag savings.

As an example, let us examine the case where $c_{l_{max}}/C_{Lmvr} = 1.05$. The optimal planform with and without maneuver load alleviation is shown in Figure 56. Stall constraints really limit the wing designed without maneuver load alleviation at this condition, forcing a span smaller than the reference wing. However, the wing designed with maneuver load alleviation is able to increase the span out to an aspect ratio of 13.5 (based on trapezoidal area of reference wing).

The large increase in span is achieved by shifting the lift inboard with maneuver load alleviation as seen in Figure 57. The c_l distributions are shown for the wing designed with and without maneuver load alleviation in Figures 58 and 59 respectively. We see that with maneuver load alleviation, the stall constraint is critical inboard at the maneuver load and critical outboard at 1g stall. For the wing designed without maneuver load alleviation, the maneuver c_l distribution is critical since it occurs at a higher C_L than does 1g stall.

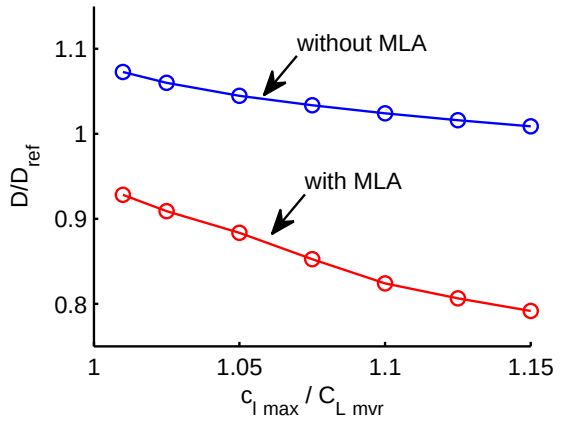

Figure 55. Drag reduction as a function of $c_{l\,max}/C_{L\,mvr}$ showing benefit of MLA

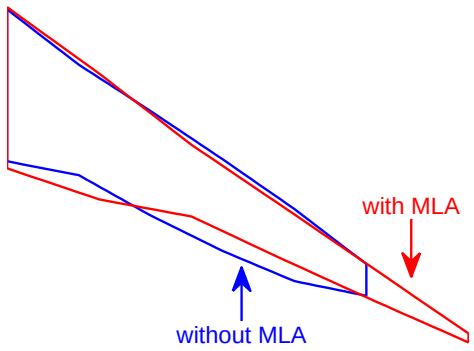

Figure 56. Optimized planform with and without MLA ($c_{l\,max}/C_{L\,mvr} = 1.05$)

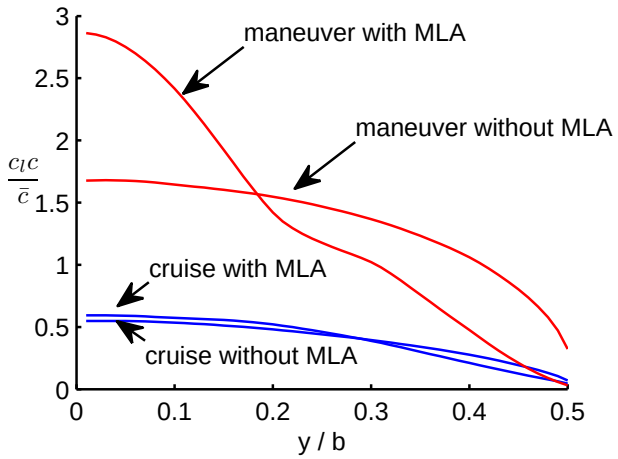

Figure 57. Optimized lift distributions ($c_{l\,max}/C_{L\,mvr} = 1.05$)

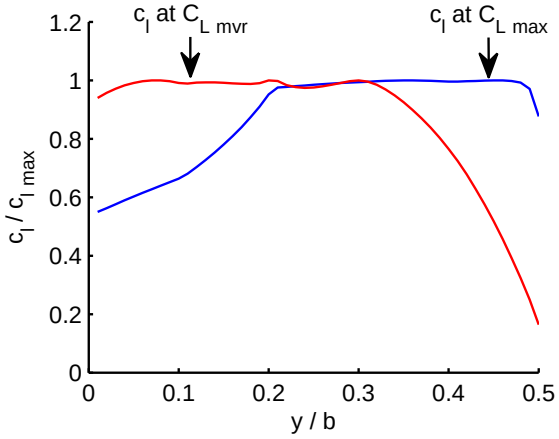

Figure 58. c_l distribution with MLA ($c_{l\,max}/C_{L\,mvr} = 1.05$)

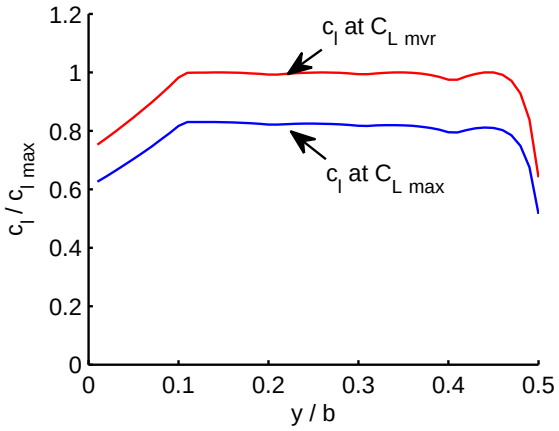

Figure 59. c_l distribution without MLA ($c_{l\,max}/C_{L\,mvr} = 1.05$)

5. Conclusion

Several important considerations in conceptual wing design were highlighted here. These include the importance of accounting for the wing structural box, viscous drag, section c_l constraints, differences in cruise C_L and maneuver C_L, wing skin thickness, and the benefit of using multidisciplinary optimization in the conceptual design phase. Some of the most significant results presented here include:

- At fixed lift, weight, and stall speed, the minimum drag trapezoidal tip device depends on the ratio of the maneuver lift coefficient to the cruise lift coefficient. For $C_{L_{mvr}}/C_L = 1$ tip extensions show a slight advantage compared with winglets, while for $C_{L_{mvr}}/C_L = 2.5$ winglets are slightly better than tip extensions. These same trends apply for wing retrofits and for new wing designs.

- C-wings have slightly lower drag compared with wings and wings with winglets when positive pitching moments are required about the aerodynamic center. This may be especially true for designs with span constraints or low sweep.

- Maneuver Load Alleviation (and Gust Load Alleviation) can offer large reductions in drag (on the order of 15% for the designs evaluated here), however an analysis of the structural dynamics is necessary for the resulting high aspect ratio designs.

These conclusions represent fundamental multidisciplinary considerations in wing design. Design decisions, however, would need to be made in the context of specific and complete design studies. For example, as pointed out by Heyson et al., it is not clear that an increase in wing weight will lead to an increase in total aircraft weight. It may be that the increase in wing weight is offset by the decrease in fuel weight due to the reduction in drag. Many more complex trade-offs exist as entire configurations and missions are optimized. Although the objective of this paper was to explore results of a more general nature, the methodology used could be applied in more specific conceptual design studies. The rapid analysis methods combined with nonlinear optimization allow for efficient exploration of large areas of the design space.

A few improvements could be made to the method highlighted here. Transonic drag rise, variation in material properties (especially in winglets), torsion-dependent weight (may be particularly important for raked tips), airfoil section design, and steady aeroelastics are a few areas that could be addressed and may yield additional insight. Some of these improvements are currently being pursued.

Acknowledgments

The authors gratefully acknowledge support from the National Defense Science and Engineering Graduate (NDSEG) Fellowship program

References

[1]Kroo, I., "Nonplanar Wing Concepts for Increased Aircraft Efficiency," *VKI lecture series on Innovative Configurations and Advanced Concepts for Future Civil Aircraft*, June 2005.

[2]Aviation Partners, I., "Aviation Partners Blended Winglets," `http://www.aviationpartners.com/`, August 2008.

[3]Hemke, P. E., "Drag of wings with end plates," NACA TR 267, National Advisory Committee for Aeronautics, 1928.

[4]Mangler, W., "The lift distribution of wings with end plates," NACA TM 856, National Advisory Committee for Aeronautics, 1938.

[5]Whitcomb, R. T., "A Design Approach and Selected Wind-Tunnel Results At High Subsonic Mounted Speeds for Winglets," NASA TN D-8260, National Aeronautics and Space Administration, July 1976.

[6]Heyson, H. H., Riebe, G. D., and Fulton, C. L., "Theoretical Parametric Study of the Relative Advantages of Winglets and Wing-Tip Extensions," NASA TP 1020, National Aeronautics and Space Administration, Sept. 1977.

[7]Flechner, S. G. and Jacobs, P. F., "Experimental results of winglets on first, second, and third generation jet transports," Tech. rep., NASA, Jan 1978.

[8]Jones, R. T. and Lasinski, T. A., "Effect of Winglets on the Induced Drag of Ideal Wing Shapes," Technical Memorandum 81230, NASA, September 1980.

[9]Kroo, I., "Design and Analysis of Optimally-Loaded Lifting Systems," *AIAA*, Vol. 84, No. 2507, Oct. 1984.

[10]Asai, K., "Theoretical Considerations in the Aerodynamic Effectiveness of Winglets," *Journal of Aircraft*, Vol. 22, No. 7, July 1985, pp. 635–637.

[11]Zimmer, H., *The Aerodynamic Optimization of Wings at Subsonic Speeds and the Influence of Wing Design*, Ph.D. thesis, University of Stuttgart, Stuttgart, Germany, 1983, Translated into English in NASA TM-88534.

[12]Slingerland, R. and Verstraeten, J. G., "Drag Characteristics for Optimally Span-loaded Planar, Wingletted, and C-wings," *46th AIAA Aerospace Sciences Meeting and Exhibit*, AIAA, Jan 2008.

[13]Weissinger, J., "The Lift Distribution of Swept-Back Wings," Technical Memorandum 1120, NACA, March 1947, Translation of Uber die Auftriebsverteilung von Pfeilflugeln Forschungsbericht Nr. 1553.

[14]Federal Aviation Regulations, *FAR Part 25*.

[15]Ning, S. A. and Kroo, I., "Tip Extensions, Winglets, and C-wings: Optimization in Conceptual Wing Design," `http://aero.stanford.edu/adgreports.html`, August 2008.

[16]Kroo, I. and Shevell, R., "Aircraft Design: Synthesis and Analysis," `http://adg.stanford.edu/aa241/AircraftDesign.html`, September 2006, Version 1.2.

[17]Grant, M. and Boyd, S., "CVX: Matlab software for disciplined convex programming (web page and software)," April 2008, `http://stanford.edu/~boyd/cvx`.

[18]Grant, M. and Boyd, S., "Graph implementations for nonsmooth convex programs," To appear in Recent Advances in Learning and Control (a tribute to M. Vidyasagar), V. Blondel, S. Boyd, and H. Kimura, editors. Springer, 2008, `http://stanford.edu/~boyd/graph_dcp.html`.

[19]Prandtl, L. and Tietjens, O. G., *Applied Hydro- and Aeromechanics*, Dover Publications, 1957.

[20]Jones, R. T., "The Spanwise Distribution of Lift for Minimum Induced Drag of Wings Having a Given Lift and a Given Bending Moment," NACA TN 2249, National Advisory Committee for Aeronautics, Dec. 1950.

[21]McGeer, T., *Wing Design for Minimum Drag with Practical Constraints*, Ph.D. thesis, Stanford University, Dec. 1983.

[22]Wakayama, S., *Lifting Surface Design Using Multidisciplinary Optimization*, Ph.D. thesis, Stanford University, Dec. 1994.

Appendix

Bending Weight Computation

Here we consider the difference between cruise loading and maneuver loading. This requires that we account for the difference in lift coefficient when computing the maneuver lift distribution and account for the difference in dynamic pressure when computing the bending weight.

Difference in Lift Coefficient

To compute the lift distribution at a different lift coefficient we would like to separate the lift distribution into a basic (twist dependent) and additional (angle of attack or C_L dependent) lift distribution. For the vortex lattice method used the circulation distribution is given by

$$[AIC]\{\gamma\} = \{bc\}$$

where

$$\{bc\} = \vec{V} \cdot \hat{n}$$

The boundary condition vector is derived below using a standard aerodynamic coordinate system aligned with the root chord of the wing. (x-aft,y-right wing, z-up). For this problem with no sideslip or angular velocity, $\vec{V}$ is given by

$$\vec{V} = \begin{pmatrix} V_\infty \cos\alpha \\ 0 \\ V_\infty \sin\alpha \end{pmatrix}$$

and using thin airfoil approximation with no camber

$$\hat{n} = \begin{pmatrix} \sin\theta \\ -\cos\theta\sin\phi \\ \cos\theta\cos\phi \end{pmatrix}$$

thus

$$\{bc\} = \cos(\alpha)\{\sin(\theta)\} + \sin(\alpha)\{\cos(\theta)\cos(\phi)\}$$

where V_∞ has been absorbed into $[AIC]^{-1}$ for convenience in the derivation.

In order to explicitly separate the basic and additional lift distribution we take a second order Taylor series approximation for the sine and cosine of the angle of attack and twist. These angles will be small

for normal configurations, thus a second order expansion should be an excellent approximation. The Taylor series expansion is given by

$$\sin(x) = x - \frac{x^3}{3!} + ...$$

$$\cos(x) = 1 - \frac{x^2}{2!} + ...$$

thus

$$\sin(x)\cos(y) \approx (x - \frac{x^3}{3!})(1 - \frac{y^2}{2!}) = x - \frac{x^3}{6} - \frac{xy^2}{2} + \frac{x^3y^2}{12}$$

assuming x and y are small and keeping only second order terms we have

$$\sin(x)\cos(y) \approx x$$

Thus we take the approximation

$$\{bc\} = \{\theta\} + \alpha\{\cos(\phi)\}$$

Although this is the same result we would get by linearizing for small angles, we see that it is actually a second order result. We can then use this approximation to eliminate the dependence on the twist distribution, which is unknown.

$$\{\gamma\}_2 = \{\gamma\}_1 + (\alpha_2 - \alpha_1)[AIC]^{-1}\{\cos(\phi)\} \tag{1}$$

To make this equation more useful let us first make it non-dimensional.

$$C_{L2} = C_{L1} + \frac{(\alpha_2 - \alpha_1)}{qS}\{LIC\}^T[AIC]^{-1}\{\cos(\phi)\} \tag{2}$$

To be absolutely clear, it was implicitly implied in the above step that C_{L2} and C_{L1} should be normalized by the same dynamic pressure. This is actually not necessary. To make this more explicit we could write $C_{L1} = \frac{L_a}{q_a S} = \frac{L_b}{q_b S}$ where a and b were two different free-stream conditions. Since lift scales with the dynamic pressure the non-dimensional quantity can be computed at any dynamic pressure. The product $LIC^T[AIC]^{-1}$ also is proportional to qS, making that term non-dimensional as well. This clarification is important to make, because as discussed previously the cruise C_L and maneuver C_L typically occur at different dynamic pressures.

We would now like to combine Equations (1) and (2) to eliminate the angle of attack dependence.

$$\{\gamma\}_2 = \{\gamma\}_1 + \frac{(C_{L2} - C_{L1})qS}{\{LIC\}^T[AIC]^{-1}\{cos(\phi)\}}[AIC]^{-1}\{\cos(\phi)\} \tag{3}$$

or to make the dependence on $\{\gamma_1\}$ explicit

$$\{\gamma\}_2 = \{\gamma\}_1 + \left(\frac{C_{L2}}{C_{L1}} - 1\right)\frac{\{LIC\}^T\{\gamma\}_1}{\{LIC\}^T[AIC]^{-1}\{cos(\phi)\}}[AIC]^{-1}\{\cos(\phi)\}$$

If we take condition 1 to be cruise, and condition 2 to be the critical maneuver load we have

$$\{\gamma_{mvr}\} = \{\gamma\} + \left(\frac{C_{L2}}{C_{L1}} - 1\right)\frac{\{LIC\}^T\{\gamma\}}{\{LIC\}^T[AIC]^{-1}\{cos(\phi)\}}[AIC]^{-1}\{\cos(\phi)\} \tag{4}$$

Difference in Dynamic Pressure

When computing weight at the maneuver load we also need to account for the difference in dynamic pressure between cruise and maneuver. For many of the problems discussed in this paper this is not really necessary because the weight is normalized by the reference weight canceling out the dynamic pressure. This *is* important however, when area-dependent weight is included and this cancellation does not occur, or when comparing multiple maneuver lift coefficients to find the critical condition. The computed bending weight is proportional to the dynamic pressure. Thus, we can define a weight coefficient that is independent of dynamic pressure.

$$C_W = \frac{W}{qSc}$$

where S and c can be any reference area and chord length. The correct weight at maneuver is now given by

$$W_{mvr} = C_W(q_{mvr}Sc) = W\frac{q_{mvr}}{q}$$

This can be re-cast in terms of the maneuver limit load factor. The load factor is given by:

$$n = \frac{L_{mvr}}{L} = \frac{C_{Lmvr}q_{mvr}}{C_L q}$$

if we substitute this into the previous equation we have

$$W_{mvr} = W\frac{n}{C_{Lmvr}/C_L}$$

Two Computation Methods

We now take a step back to discuss how the weight is actually computed. If we consider a section of the wing structural box the local bending moment is given by:

$$M_b = \sigma\frac{A}{2}t$$

where σ is the stress, and t the airfoil thickness. If the wing is fully stressed then σ will be the yield stress. The weight of stressed material in the semi-span of the wing can be found by integrating along the semi-span.

$$W_b = \rho_{material}\int Ads = \rho_{material}\int \frac{2M_b}{\sigma_{yield}t}ds$$

The bending weight of the wing should then be proportion to the index

$$I_b = \int \frac{M_b}{t}ds$$

The discretization of this integral involves a double sum.

$$I_b = \sum_i\sum_j \frac{\rho V_\infty \gamma_j ds_j R_{ij} ds_i}{\frac{t}{c}c_i}$$

where R_{ij} is the local moment arm for all elements that are structurally connected. This double sum can be computed by summing over i first or by summing over j first. The first case is particularly useful in the trade studies where the geometry is fixed and the lift distribution is optimized. The second case is necessary for problems like C-wings where the optimal lift distribution may produce negative bending moments at some sections.

Summing over i first is convenient for the problems where we are computing optimal load distributions. This is the method described by Kroo[9] and built upon here. For these problems it is convenient to separate the calculation of the aerodynamic performance into a part due to the geometry and a part due to the load distribution. This allows us to define the weight as the dot product of two vectors $W = \{WIC\}^T\{\gamma\}$. Using equation 4, and accounting for the difference in dynamic pressure, the weight at maneuver is given by:

$$\begin{aligned} I_b &= \frac{n}{C_{Lmvr}/C_L}\{WIC\}^T\{\gamma_{mvr}\} \\ &= \frac{n}{C_{Lmvr}/C_L}\{WIC\}^T\{\gamma\} + n\left(1 - \frac{1}{C_{Lmvr}/C_L}\right)\frac{\{WIC\}^T[AIC]^{-1}\{cos(\phi)\}}{\{LIC\}^T[AIC]^{-1}\{cos(\phi)\}}\{LIC\}^T\{\gamma\} \end{aligned}$$

This is still a linear function of the circulation distribution $\{\gamma\}$. Thus we can use the exact same optimization framework as shown by Kroo if we replace the weight influence coefficient matrix as follows:

$$\{WIC\} \leftarrow \frac{n}{C_{Lmvr}/C_L}\{WIC\} + n\left(1 - \frac{1}{C_{Lmvr}/C_L}\right)\frac{K_W}{K_L}\{LIC\}$$

where

$$K_L = \{LIC\}^T [AIC]^{-1} \{cos(\phi)\}$$

and

$$K_W = \{WIC\}^T [AIC]^{-1} \{cos(\phi)\}$$

The only thing we need to specify is the ratio $\frac{C_{Lmvr}}{C_L}$.

The second method for computing the bending weight is necessary when the local bending moment may be negative at some sections. For this case we cannot use $\{WIC\}$ because it does not give the correct distribution of local bending moment, nor does it give the correct solution if the bending moment is negative at any section. This is because the amount of stressed material actually depends upon the absolute value of the local bending moment.

$$I_b = \int \frac{|M_b|}{t} ds$$

The discretized version is given as:

$$I_b = \frac{n}{C_{Lmvr}/C_L} \sum_i \left| \sum_j \frac{\rho V_\infty \gamma_{mvrj} ds_j R_{ij} ds_i}{\frac{t}{c} c_i} \right|$$

To simplify the notation in the paper we will refer to computation more generically as

$$I_b = \left|\left| \left\{ \frac{M_b}{t} ds \right\} \right|\right|_1$$

This emphasizes the need to take the absolute value of the bending moment, with the understanding that the computation must account for the difference in lift coefficient and dynamic pressure as outlined here.

Stall Speed Computation

We start with Equation (3) from the previous section and set condition 1 as cruise and condition 2 as stall.

$$\{\gamma\}_{max} = \{\gamma\} + \frac{(C_{Lmax} - C_L) qS}{\{LIC\}^T [AIC]^{-1} \{\cos(\phi)\}} [AIC]^{-1} \{\cos(\phi)\}$$

or in terms of $\{c_l\} = \frac{2\{\gamma\}}{U\{c\}}$

$$\{c_l\}_{max} = \{CLIC1\} \circ \{\gamma\} + \{CLIC0\}$$

where

$$\{CLIC1\} = \frac{2}{U\{c\}}$$

and

$$\{CLIC0\} = \frac{\rho US(C_{Lmax} - C_L)}{\{LIC\}^T [AIC]^{-1} \{\cos(\phi)\}} \frac{[AIC]^{-1} \{\cos(\phi)\}}{\{c\}}$$

Note that the term $\{CLIC1\} \circ \{\gamma\}$ is not a scalar dot product but an element by element product (i.e. $c(i) = a(i)b(i)$). Similarly, the last term in $\{CLIC0\}$ is an element by element division.